University of Cologne

Faculty of Mathematics and Science
Institute of Theoretical Physics

Bachelor Thesis

Thermalization and Integrability in the one-dimensional Bose-Hubbard Model

Author: Marvin Pinkwart

First Examiner: Prof. Dr. Achim Rosch

Second Examiner: Prof. Dr. Simon Trebst

Submission Date: 17.07.2014

Matriculation Number: 5415438

Abstract

The one-dimensional Bose-Hubbard model is a model which is suited for the description of optical lattices whereby properties of solids can be investigated experimentally in an idealized form. After a quantum quench, which is a fast change of the parameters of the Hamiltonian, the system is not in an eigen state and thus relaxes temporally into an equilibrium state. The observed quench is characterized by a change of the attractive interaction parameter J between lattice sites from a vanishing value up to a small but finite value. The repulsive interaction parameter U between particles on one site is chosen sufficiently large so that $U \gg J$. This quench can be experimentally realized by variaton of the optical lattice's potential depth. As a result of the quench quasi-particles are formed, i.e. excitations which are caused by particles hopping from one site to another, whose dynamics afterwards can be simulated regarding a semi-classical description [1]. In this case quasi-particles collide ballistically with respect to energy conservation and restricted momentum conservation, i.e. modulo 2π, which rules famously in lattices. In [2] this model has been investigated in the case of closed systems and with one particle per site and it emerged that the temporal behavior of two quantities, namely the energy correlations $\langle e_i e_{i+n} \rangle$ of quasi-particles at sites i and $i+n$ and $\langle \cos(2q) \rangle$, a quantity that is closely related to the shape of the momentum distribution, can be especially well described by hydrodynamics for long times. Thereby particularly in one dimension pronounced long-time tails develop, i.e. $\sim t^{-1/2}$. In [3] the model has been investigated for open sytems by exchanging particles at a given rate.
In this thesis the number of particles per site previous to the quench is increased so that eventually the masses of the created quasi-particles approach each other and therefore the system approaches an integrable point. It will also be simulated the case with truely same masses.
It will be shown that long-time tails in their pure form do not occur until bigger times. While it is sufficient to correct the tails for one particle per site and mid-level times with $t^{-3/4}$, it will be necessary to consider further corrections when using more particles per place. Furthermore it will be shown that it would be expected that the energy correlation pursues zero exponentially regarding same masses but numerically a slower progression is observed. The momentum distribution relaxes at first with $e^{-\Gamma t}$ and $\Gamma \sim N^{-1.75}$. For same masses there is no relaxation of this quantity. At long last prefactors near equilibrium are compared for constant mass ratios.
In chapter 1 it will be dwelled on the theoretical foundations such as thermalization, integrability and second quantization. In chapter 2 the theoretical results from [2] will be reproduced and finally in chapter 3 the results are presented.

Kurzfassung

Das eindimensionale Bose-Hubbard Modell ist ein Modell, welches sich für eine einfache Beschreibung optischer Gitter eignet, mithilfe derer sich Eigenschaften von Festkörpern in idealisierter Form experimentell untersuchen lassen. Nach einem Quanten Quench (das ist eine schnelle Änderung eines Parameters im Hamilton-Operator) befindet sich das System nicht in einem Eigenzustand und relaxiert folglich zeitlich in den Gleichgewichtszustand. Der betrachtete Quench im Bose-Hubbard Modell zeichnet sich durch Änderung des attraktiven Wechselwirkungsparameters J zwischen Gitterplätzen von verschwindenem Wert hin zu einem kleinen aber endlichen Wert aus. Die repulsive Wechselwirkung U auf Gitterplätzen wird so groß gewählt, dass sie gegenber der attraktiven dominiert. Dieser Quench kann experimentell durch Variation der Potentialtiefe des optischen Gitters realisiert werden. Bei dem Quench bilden sich Quasi-Teilchen, also Anregungen, bedingt durch Hüpfen eines Teilchens auf einen benachbarten Platz, deren Dynamik darauffolgend mit einer semi-klassischen Beschreibung simuliert werden kann [1]. Hierbei stoßen die Quasi-Teilchen ballistisch unter Beachtung von Energieerhaltung und eingeschränkter Impulserhaltung, welche bekanntlich in Gittern vorherrscht. In [2] wurde dieses Modell bereits für abgeschlossene Systeme allgemein mit einem Teilchen pro Gitterplatz behandelt und es stellte sich heraus, dass die zeitliche Entwicklung zweier Größen, namentlich die Energiekorrelationen $\langle e_i e_{i+n} \rangle$ von Quasi-Teilchen auf Plätzen i und $i+n$ und $\langle cos(2q) \rangle$, eine Größe, die mit der Breite der Impulsverteilung korrespondiert, für große Zeiten besonders gut durch Hydrodynamik beschrieben werden können . Dabei entwickeln sich besonders in einer Dimension ausgeprägte long-time tails, dies bedeutet eine zeitliche Entwicklung $\sim t^{-1/2}$. In [3] wurde das Modell für offene Systeme untersucht, wobei Teilchen mit einer bestimmten Rate ausgetauscht wurden.
In dieser Arbeit soll es darum gehen, die Anzahl der Teilchen, welche sich vor dem Quench auf einem Gitterplatz befinden, zu erhöhen, sodass sich schließlich die Massen der erzeugten Quasiteilchen einander annähern und sich das System einem integrablen Punkt nähert. Es wird auch der Fall genau gleicher Massen simuliert werden.
Man wird sehen, dass long-time tails in reiner Form erst für größere Zeiten auftreten. Während es für ein Teilchen pro Gitterplatz genügt, die tails für mittlere Zeiten mit $t^{-3/4}$ zu korrigieren, werden bei mehreren Teilchen pro Platz weitere Korrekturen notwendig. Weiterhin wird sich zeigen, dass zu erwarten wäre, dass die Energiekorrelation für gleiche Massen exponentiell gegen Null strebt, sich numerisch aber ein langsamerer Verlauf ergibt. Die Impulsverteilung relaxiert zunächst mit $e^{-\Gamma t}$ mit $\Gamma \sim N^{-1.75}$. Bei gleichen Massen der Quasi-Teilchen ergibt sich hier keine Relaxation. Zu guter Letzt werden Vorfaktoren nahe des Gleichgewichts für konstantes Massenverhältnis verglichen.
In Kapitel 1 der Arbeit wird auf theoretische Grundlagen, wie beispielsweise Thermalisierung, Integrabilität und die zweite Quantisierung eingegangen. In Kapitel 2 werden dann die analytischen Ergebnisse aus [2] für den betrachteten Quench reproduziert. Schließlich werden in Kapitel 3 die Ergebnisse präsentiert.

Contents

List of Figures

1 Theoretical Foundations

1.1 Optical Lattices

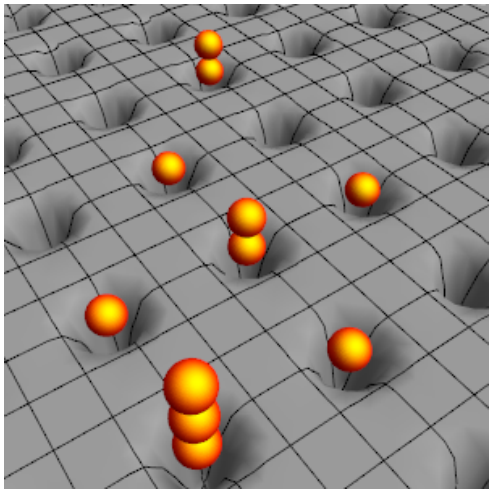

Figure 1: *Schematic image of a bosonic gas in a two-dimensional optical lattice*

Optical lattices nowadays represent a powerful instrument for the investigation of idealized solid state quantum models. The possibility of modulating various parameters as the potential height or the geometry of the lattice and the good environmental screening count among their biggest advantages. For all real solids are susceptible to unwanted outside influences and correlations in between the solid optical lattices establish a new world of experimental possibilities and allow to focus on certain problems of systems in purity. Mostly dilute, ultra cold fermionic or bosonic gases of neutral atoms are studied by the use of optical lattices. One theoretical quantum model well suited for experimental studies with optical lattices is the Bose-Hubbard model which will be investigated numerically in this thesis.

An optical lattice is produced by interfering laser beams which form a periodic potential. The potential results from interaction between the periodic oscillating electric field of the laser and the induced oscillating dipole moment in the atom [4]

$$V(\vec{r}) = -\vec{d} \cdot \vec{E}(\vec{r}) \sim \alpha(\omega_L)|\vec{E}(\vec{r})|^2 \quad . \tag{1.1}$$

In this case α denotes the atoms polarizability. As the lasers intensity $I(\vec{r})$ is proportional to $|\vec{E}(\vec{r})|^2$ the potential height can be directly manipulated by changing the light intensity. The reason for the dipole-field coupling leading to a potential is the AC-Stark effect which leads to an energy-splitting when coupling an dipole to an oscillating field.

To avoid spontaneous emission or absorption one adjusts the lasers frequency ω_L so that $\omega_L \gg \omega_{resonance}$ (which yields to a repulsive potential as the atoms are located at the potential hills) or $\omega_L \ll \omega_{resonance}$ (which yields to an attractive potential as the atoms are located at the potential valleys). Optical lattices are usually cooled so that losses of particles become very rare. Nevertheless particle losses can never be excluded completely. For a study on such losses see [3].

In one dimension two opposing laser beams form a standing wave. The resulting potential's period is given by half the laser's wavelength. One can also obtain two-dimensional lattices by using perpendicular stationary waves that allow movement along a one-dimensional tube. Those tubes then build up a two-dimensional array. A three-dimensional lattice is achieved by three perpendicular standing waves.

One can change the lattice's geometry from an rectangular geometry to many fancy ones by using laser beams which are not quite collinear for interference.

1.2 Second Quantization

1.2.1 From First to Second Quantization

Let us briefly recapitulate the basics of quantum mechanics and then introduce the formalism of second quantization which is way more proper for the description of many-particle quantum systems than the formalism of basic single-particle quantum mechanics.

In single-particle quantum mechanics one works in the complete and separable Hilbert space $\mathcal{H}$ in which a single-particle quantum state is represented by a ray, i.e the one-dimensional linear combination of a vector. Two choices of a special vector space are mostly used, i.e. the Schrödinger picture and the Heisenberg picture. The big difference lies in the time-dependency of states and operators. While in Schrödinger picture the states themselves are time-dependent and operators can carry maximally an explicit time dependency, the states in the Heisenberg picture are time-independent whereas operators carry a time-dependency (which can be implicit). Operators can be transformed from one into the other picture by considering the time-dependent Schrö dinger equation and an invariant expectation value

$$\hat{H}|\Psi\rangle_t = i\hbar\partial_t|\Psi\rangle_t \tag{1.2}$$

$$\Leftrightarrow \quad |\Psi\rangle_t = e^{-\frac{i}{\hbar}\hat{H}t}|\Psi_0\rangle$$

$$\overset{!}{\Rightarrow} \quad {}_t\langle\Psi|\hat{O}_{schr}|\Psi\rangle_t = \langle\Psi|\hat{O}_{heis}(t)|\Psi\rangle$$

$$\Rightarrow \quad \hat{O}_{heis}(t) = e^{\frac{i}{\hbar}\hat{H}t}\hat{O}_{schr}e^{-\frac{i}{\hbar}\hat{H}t} \quad . \tag{1.3}$$

Hereafter we will always refer to the Schrödinger picture. In this case the norm $|\Psi(x)|^2$ represents the probability density of finding the particle in state Ψ at place x.

Every physical transformation $\hat{T}$ has to be unitary in order to preserve the quantum state's norm. If an operator $\hat{O}$ corresponds to a real physical observable it has to be self-adjoint so that the expectation value $\langle\Psi|\hat{O}|\Psi\rangle$ is a real number.
In general a quantum state can be a linear combination of eigenstates $|n\rangle$ of the Hamilton operator $\hat{H}$

$$|\Psi\rangle = \sum_n c_n|n\rangle \quad . \tag{1.4}$$

When the energy is measured the state collapses and transitions into the eigenstate $|n\rangle$ with probability $|c_n|^2$. In real experiments it is nearly impossible to measure energies directly, especially concerning many-particle systems. It is usual to measure expectation values instead.

To describe two-particle systems one introduces the two particle state $\langle x_1, x_2|\Psi_{1,2}\rangle = \langle x_1|\lambda_1\rangle \otimes \langle x_2|\lambda_2\rangle$ with normalized energy eigenstates λ_1 and λ_2. For identical particles it is a fundamental assumption that they are indistinguishable. Regarding the permutation operator $\hat{P}$ this means $\hat{P}^2 = 1$ and so its eigenvalues are ± 1. Therefore a many particle state can either be symmetric (bosons) or antisymmetric (fermions). (Indeed in two dimensions quasi-particles, namely anyons, that are neither symmetric nor antisymmetric exist.[5]) For an N-particle system with normalized eigenstates $\lambda_i, \quad i = 1, \ldots, N$ and $\xi_{B/F} := \pm 1$ the resulting state with respect to normalization is [6]

$$|\lambda_{1,\ldots,N}\rangle = \frac{1}{\sqrt{N! \prod_{\lambda=0}^{\infty} n_\lambda!}} \sum_{\sigma} \xi^{(1-\mathrm{sign}(\sigma))/2} |\lambda_{\sigma(1)}\rangle \otimes \cdots \otimes |\lambda_{\sigma(N)}\rangle \tag{1.5}$$

where the summation runs over all permutations σ and n_λ denotes the number of particles in state λ. This state lives in the new Hilbert space

$$\mathcal{F}_N = \mathcal{H}^N = \underbrace{\mathcal{H} \otimes \ldots \otimes \mathcal{H}}_{\text{N times}} \quad . \tag{1.6}$$

One can easily imagine that for the most systems it seems nearly impossible to find all eigenstates and construct a state as given in (1.5). That is where second quantization comes in and simplifies the work.

1.2.2 Fock Space, Annihilation and Creation Operators

From now on we discard the thought of working with all the individual wave functions and introduce the description by occupation numbers. When looking at a many-particle state the main information one receives is how many particles occupy each basis state, which does not have to be an energy eigenstate. Eigenstates of various operators can be used. In this form one can write the basis states of the newly formed Hilbert space $\mathcal{F}_N$ as $|n_1, n_2, \ldots\rangle$. There is no more need for restricting the particle number to a fixed N. So one introduces the final Hilbert space which is known as the Fock space

$$\mathcal{F} = \bigoplus_{N=0}^{\infty} \mathcal{F}_N \tag{1.7}$$

with the vacuum space $\mathcal{F}_0$ of vacuum states. Every state in $\mathcal{F}$ can now be written as a linear combination of basis states

$$|\Psi\rangle = \sum_{n_1, n_2, \ldots} c_{n_1, n_2, \ldots} |n_1, n_2, \ldots\rangle \quad . \tag{1.8}$$

From now on, for simplicity, we will focus on bosons because they are the particles of interest in the Bose-Hubbard model.
It appears to be expedient to introduce a linear operator acting on Fock space and its Hermitian

adjoint, namely the (bosonic) creation and annihilation operator

$$\text{creation operator:} \qquad \hat{a}_i^\dagger |n_1, \ldots, n_i, \ldots\rangle := \sqrt{n_i + 1}\,|n_1, \ldots, n_i + 1, \ldots\rangle \tag{1.9}$$

$$\text{annihilation operator:} \qquad \hat{a}_i |n_1, \ldots, n_i, \ldots\rangle := \sqrt{n_i}\,|n_1, \ldots, n_i - 1, \ldots\rangle. \tag{1.10}$$

Their names are very suggestive for they create/annihilate a particle at state $|n_i\rangle$. One may recognize these from the algebraical solution of the harmonic oscillator. While there they were introduced only for algebraical reasons they now receive a more fundamental meaning. From the definition (1.9) one can easily confirm that

$$|n_1, n_2, \ldots\rangle = \prod_i \frac{(\hat{a}_i^\dagger)^{n_i}}{\sqrt{n_i!}} |0\rangle \tag{1.11}$$

with the single vacuum state $|0\rangle$. This way the basis of the Fock space can easily build up by frequent use of the creation operator on the vacuum state. Using the annihilation operator on this state gives 0.
Both operators satisfy the following commutation relations

$$[\hat{a}_i, \hat{a}_j^\dagger] = \delta_{ij} \quad , \quad [\hat{a}_i, \hat{a}_j] = 0 = [\hat{a}_i^\dagger, \hat{a}_j^\dagger] \quad . \tag{1.12}$$

At last we introduce the occupation number operator

$$\begin{cases} \hat{n}_i := \hat{a}_i^\dagger \hat{a}_i \\ \hat{n}_i |n_1, \ldots, n_i, \ldots\rangle = n_i |n_1, \ldots, n_i, \ldots\rangle \end{cases} \tag{1.13}$$

which counts the number of particles occupying the i^{th} state.

We now consider two different one-particle bases $|i\rangle$ and $|j\rangle$ and based on eq. (1.11) we write $|i\rangle \equiv \hat{a}_i^\dagger |0\rangle_i$. As the Hilbert space per definition is complete one can write the relation of completeness as

$$\mathbb{1} = \sum_i |i\rangle\langle i| \quad . \tag{1.14}$$

By adapting the unity operator on a basis state $|j\rangle$ one can write this state as

$$|j\rangle = \sum_i \langle i|j\rangle |i\rangle \quad . \tag{1.15}$$

This allows us to transform the annihilation and creation operators given in the basis $|i\rangle$ such that they are given by $|j\rangle$

$$\begin{aligned}\hat{a}_j^\dagger|0\rangle_j = |j\rangle &\overset{(1.14)}{=} \sum_i \langle i|j\rangle|i\rangle \\ &= \sum_i \langle i|j\rangle \hat{a}_i^\dagger|0\rangle_i \quad .\end{aligned}$$

Since there exists only one single vacuum state one can set $|0\rangle_i \equiv |0\rangle_j$ which leads to the both operators' new expressions

$$\hat{a}_j^\dagger = \sum_i \langle i|j\rangle \hat{a}_i^\dagger \tag{1.16}$$

$$\hat{a}_j = \sum_i \overline{\langle j|i\rangle} \left(\hat{a}_i^\dagger\right)^\dagger = \sum_i \langle j|i\rangle \hat{a}_i \tag{1.17}$$

1.2.3 One- and Two-Particle Operators

The last step of this section is the representation of one- and two-particle operators with the new language of second quantization. We will see that a single-particle operator can be written as a sum over creation and annihilation operators weighted with a coefficient. As we showed how to transform those in the last section we may first focus on a one-particle operator that is diagonal in a certain basis $|i\rangle$ and transform to an arbitrary basis later on. Let the operator be called $\hat{\mathcal{U}}_1$ and as it is assumed to be diagonal one can write it as

$$\hat{\mathcal{U}}_1 = \sum_i \langle i|\hat{u}|i\rangle|i\rangle\langle i| =: \sum_i u_i|i\rangle\langle i| \tag{1.18}$$

where $\hat{u}_i$ acts just on the i$^{\text{th}}$ particle. With the Notation $|n\rangle \equiv |n_1, n_2, \ldots\rangle$ this yields to

$$\begin{aligned}\langle\bar{n}|\hat{\mathcal{U}}_1|n\rangle &= \sum_i u_i n_i \langle\bar{n}|n\rangle \\ &= \langle\bar{n}| \sum_i u_i \hat{n}_i |n\rangle\end{aligned}$$

and since the choice of $|\bar{n}\rangle$ and $|n\rangle$ is absolutely free it follows that

$$\hat{\mathcal{U}}_1 = \sum_i u_i \hat{n}_i = \sum_i \langle i|\hat{u}|i\rangle \hat{a}_i^\dagger \hat{a}_i \quad . \tag{1.19}$$

Recalling eq. (1.16) one can easily transform to an arbitrary non-diagonal basis and achieve the most general second quantized representation of the one-particle operator

$$\hat{\mathcal{U}}_1 = \sum_{ij} \langle i|\hat{u}|j\rangle \hat{a}_i^\dagger \hat{a}_j \quad . \tag{1.20}$$

It turns out that a two-particle operator can be written very similar

$$\hat{\mathcal{U}}_2 = \sum_{i,j,l,k} \langle i,j|\hat{u}_2|l,k\rangle \hat{a}_i^\dagger \hat{a}_j^\dagger \hat{a}_k \hat{a}_l \quad . \tag{1.21}$$

1.3 Thermalization

This section is based on [7].

In classical mechanics thermalization is closely related to the concept of ergodicity. An ergodic Hamiltonian offers the system the possibility of thermalization. Let us consider a d-dimensional system with N degrees of freedom, so that the system at a certain time t can be described as a point in the $2dN$-dimensional phase space $\mathcal{P} = \{(p,q)\}$, i.e. the space of generalized coordinates, which in the simplest case is isomorphic to $\mathbb{R}^{dN} \times \mathbb{R}^{dN}$. Energy conservation $\mathcal{H}(p(t),q(t)) = E(t) \equiv E_0 \quad \forall t > 0$ restricts the system to a $(dN-1)$-dimensional sub-manifold of $\mathcal{P}$ which means to a hyperplane. Starting with an initial condition (p_0, q_0) and energy conservation, the Hamiltonian is said to be ergodic when the solutions of the Hamilton equations uniformly cover every single point in this hyperplane.
If this prerequisite is fulfilled one can define thermalization of an observable $\mathcal{O}$, which means that its long time average equals the micro canonic expectation value

$$\begin{aligned} \langle \mathcal{O} \rangle_{lt} &= \lim_{T\to\infty} \frac{1}{T} \int_0^T \mathrm{d}t\, \mathcal{O}(p(t),q(t)) \\ &= \langle \mathcal{O} \rangle_{micro} = \frac{\int \mathrm{d}q^{dN} \mathrm{d}p^{dN}\, \mathcal{O}(p,q)\delta(\mathcal{H}(p,q) - \mathcal{H}(p_0,q_0))}{\int \mathrm{d}q^{dN} \mathrm{d}p^{dN}\, \delta(\mathcal{H}(p,q) - \mathcal{H}(p_0,q_0))} \quad . \end{aligned} \tag{1.22}$$

In the thermalized state the system is temporally stationary on a macroscopical level, i.e. considering expectation values. It can be described by few macroscopic thermodynamic variables such as volume, pressure, entropy, etc. Well known statistical mechanics are appropriate to describe those stationary states. It can be shown that all thermodynamic ensembles describe the thermalized system equally except for fluctuations.

The definition for quantum system looks quite similar. Local operators thermalize if the long-time average of their expectation values converge to a (micro/macro-)canonical one

$$\langle \hat{\mathcal{O}} \rangle_{lt} = \lim_{T\to\infty} \frac{1}{T} \int_0^T \mathrm{d}t\, \langle \Psi(t)|\hat{\mathcal{O}}(x)|\Psi(t)\rangle \to \langle \mathcal{O}(x)\rangle_{can} = \frac{\mathrm{Tr}\left[e^{-\beta\mathcal{H}}\hat{\mathcal{O}}(x)\right]}{Z} \tag{1.23}$$

with the partition function $Z = \mathrm{Tr}\left[e^{-\beta\mathcal{H}}\right]$. In this case β can be determined using

$$E(t) \equiv E_0 = \frac{\mathrm{Tr}\left[e^{-\beta\mathcal{H}}\mathcal{H}\right]}{Z} \quad \forall t > 0$$

where $E(t)$ denotes the Hamilton operator's expectation value.
Quantum ergodicity is a difficult topic and strict ergodicity almost never is reached. However, the Eigenstate Thermalization Hypothesis (ETH) implies that in most quantum systems observable operators should thermalize. The main idea is the following:

Let the initial quantum state be given by a linear combination of energy eigenstates $|\phi\rangle$

$$|\Psi(0)\rangle = \sum_n c_n |\phi_n\rangle \quad .$$

The state temporally evolves into the new state

$$|\Psi(t)\rangle = \sum_n c_n e^{-itE_n/\hbar} |\phi_n\rangle \quad .$$

Now consider an operator $\hat{\mathcal{O}}$ and write its matrix element as $\langle\phi_m|\hat{\mathcal{O}}|\phi_n\rangle =: \mathcal{O}_{mn}$. Its expectation value is therefore given by (supposing non-degeneracy)

$$\langle\hat{\mathcal{O}}(t)\rangle = \sum_n |c_n|^2 \mathcal{O}_{nn} + \sum_{m\neq n} \bar{c}_m c_n e^{i(E_m-E_n)t/\hbar} \mathcal{O}_{mn} \quad . \tag{1.24}$$

The long-time average (1.23) becomes

$$\langle\hat{\mathcal{O}}\rangle_{lt} = \sum_n |c_n|^2 \mathcal{O}_{nn} \quad .$$

The second term in (1.24) vanishes because $|e^{-i(E_m-E_n)t/\hbar}|_{\mathbb{C}} = 1 \ \forall t$ and therefore it is $\lim_{T\to\infty} \frac{|e^{-i(E_m-E_n)T/\hbar}-1|}{T} = 0$. Now consider a small energy shell $\mathcal{S} = [E, E+\Delta E)$. The main prediction of the ETH is the approximate constancy of $\mathcal{O}_{nn} \approx \mathcal{O}_{\mathcal{S}}$ for $E_n \in \mathcal{S}$. In closed systems energy is conserved and therefore $|c_n| \approx 0$ for $E_n \notin \mathcal{S}$. Supposing the constancy prediction is true it leads to

$$\begin{aligned} \langle\hat{\mathcal{O}}\rangle_{lt,\mathcal{S}} &\approx \sum_{\mathcal{S}} |c_n|^2 \mathcal{O}_{\mathcal{S}} = \mathcal{O}_{\mathcal{S}} \sum_{\mathcal{S}} |c_n|^2 = \mathcal{O}_{\mathcal{S}} \\ &= \frac{1}{\mathcal{N}} \sum_{\mathcal{S}} \mathcal{O}_{\mathcal{S}} \approx \frac{1}{\mathcal{N}} \sum_{\mathcal{S}} \mathcal{O}_{nn} \\ &= \langle\hat{\mathcal{O}}\rangle_{micro} \end{aligned} \tag{1.25}$$

where $\mathcal{N}$ denotes the number of energy eigenstates in $\mathcal{S}$. So the quintessence is: observables' expectation values with respect to a single energy eigenstate are predicted to be approximately the microcanonic expectation value and as a consequence the expectation value with respect to any initial state becomes the microcanic one for long times.
There is no analytical proof for the ETH but it has been investigated numerical several times and been proven for many systems, e.g. in [8]. A system needs to be non-integrable and the observables need to have a thermodynamical limit in order to be supposed to satisfy the ETH.

It has to be said that the thermalization of an operator does not imply the thermalization of other operators of the same system. So which operators can thermalize ? This leads us again to quantum ergodicity and the von Neumann ergodic theorem. The main statement is that considering a finite family of coarse grained (i.e. just a small subset of all possible operators) commuting operators $\mathcal{M}_l$ representing macroscopic observables those operators will thermalize for the most times and the most choices of $\{\mathcal{M}_l\}$ where "most" regarding unitary operators means that the so called Haar measure μ satisfies the relation $\mu(\{\mathcal{M}_l\}) \geq 1-\delta$ with a certain $0 < \delta \ll 1$ and regarding time that the following relation is satisfied :

$$\lim_{T\to\infty} \inf \frac{1}{T}\lambda\left(\{0 < t < T | \text{thermalization relation is satisfied at time t}\}\right) \geq 1-\delta$$

where λ denotes the Lebesgue measure on the relevant subset of $\mathbb{R}$. For a far more detailed discussion see [9].

1.4 Quantum Quenches

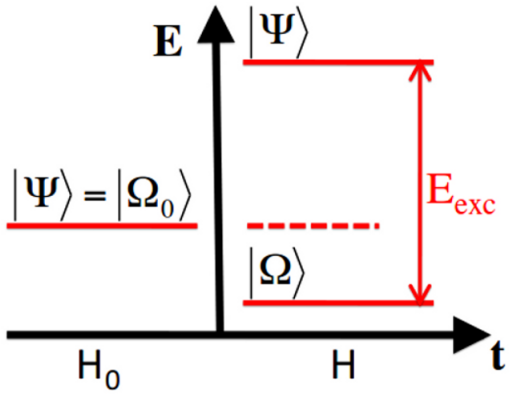

Figure 2: *Ground state* $|\Omega_0\rangle$ *of Hamiltonian* $\mathcal{H}_0$ *, ground state* $|\Omega\rangle$ *of* $\mathcal{H}_1$ *and excited state* $|\Psi\rangle = |\Psi\rangle_{ini}$ *, taken from [10]*

Quantum quenches are probably the easiest way of preparing a many-body quantum system in an out of equilibrium state and investigate the time evolution towards a thermalized state or in case of e.g. integrable systems observe if certain quantities reach a thermalized state. They are often applied to experiments on ultra cold atoms in optical lattices which minimizes environmental coupling and therefore avoids large decoherence or dissipation. A quantum quench is defined as a change of certain parameters of the Hamilton operator, i.e. a weak or strong perturbation,

$$\mathcal{H}(\alpha) \to \mathcal{H}(\tilde{\alpha} \neq \alpha) \tag{1.26}$$

or in some cases equivalently

$$\mathcal{H}_0 \to \mathcal{H}_1 = \mathcal{H}_0 + \lambda \mathcal{W} \tag{1.27}$$

which can be done "instantaneously" (in reality one can only do it very fast) or slowly (mostly slow quenches are not referred to as quenches). Normally the system before the quench is prepared in the ground state of $\mathcal{H}_0$. Therefore slowly changing parameters are usually not of interest as the system can follow this change and stays in the ground state. After the quench the system is situated in an excited state $|\Psi\rangle_{ini}$ which is a linear combination of eigenstates of $\mathcal{H}_1$ and evolves unitarily in time with the time evolution operator build by the new Hamiltonian $\mathcal{H}_1$. Usually one studies closed systems and following energy conservation the system cannot relax towards the ground state of $\mathcal{H}_1$. So after $|\Psi\rangle_{ini}$ has built up after a very short time the next step is to generate quasi-particles which will interact later on. Those interactions, mostly scattering, can lead to global thermalization. Transport quantities often relax quite slowly for conserved quantities as energy density have to be transported over partly large distances since spatial fluctuations are often pronounced directly after the quench.

1.5 Integrability

1.5.1 Classical Definition

In classical physics integrability is a well known and understood concept. Let a classical system with f degrees of freedom be given and use the Hamilton formalism. The Poisson brackets of two functions $F, G : \mathcal{P} \to \mathbb{R}$ are defined by

$$\{F, G\} = \sum_{i=1}^{f} \left(\frac{\partial F}{\partial q_i} \frac{\partial G}{\partial p_i} - \frac{\partial G}{\partial q_i} \frac{\partial F}{\partial p_i} \right) \quad . \tag{1.28}$$

For $G \equiv \mathcal{H}$, concerning the Hamilton equations, this becomes

$$\{F, \mathcal{H}\} = \frac{\mathrm{d}F}{\mathrm{d}t} \quad .$$

Thus a quantity $\mathcal{I}$ is temporally conserved if $\{\mathcal{I}, \mathcal{H}\} = 0$ and is called a constant of motion. If there exist f of those constants that are functionally independent, i.e. their gradients are linearly independent, and satisfy $\{\mathcal{I}_i, \mathcal{I}_j\} = 0$ one can now find new generalized momenta $\{p_i\}$, $i = 1, \ldots, f$ which are as well constants of motion since

$$\frac{\mathrm{d}p_i}{\mathrm{d}t} = \sum_{j=1}^{f} \frac{\partial p_j}{\partial \mathcal{I}_j} \dot{\mathcal{I}}_j = 0 \quad .$$

Therefore the to $\{p_i\}$ corresponding generalized coordinates have to be cyclic. Cyclic coordinates allow us to easily solve the Hamilton equations

$$q_i = a_i t + b_i t \ , \ p_i = a_i \quad \Leftarrow \quad \begin{cases} \dot{p}_i = -\dfrac{\partial \mathcal{H}}{\partial q_i} = 0 \\ \dot{q}_i = \dfrac{\partial \mathcal{H}}{\partial p_i} = a_i = \text{const} \end{cases} \ . \tag{1.29}$$

A system with such f constants of motion is called integrable. The trajectories of this system evolve on a f-dimensional torus.
Very simple examples for integrable classical systems are (coupled) harmonical oscillators or the central force problem.

1.5.2 Quantum Integrability

In quantum mechanics it is way more difficult to define integrability. In [11] the most common definitions of quantum integrability have been summarized and sceptically examined. Those are:

1. One can approach quantum integrability simple-hearted and replace both the phase space functions $\mathcal{I}_i$ by quantum mechanical operators and the classical Poisson bracket by the commutator $i[,]/\hbar$ and subsequently apply the classical definition. This appears to be insufficient as the family of operators $\{|\psi_\alpha\rangle\langle\psi_\alpha\rangle\}_\alpha$ with non-degenerate energy eigenstates $|\psi_\alpha\rangle$ is a family of commuting constants of motion with the same dimension as the Hilbert space and thus every quantum system seems to be integrable. (Indeed there exist exceptions. In [7] it has been shown that "for relativistic field theory in 1+1 dimension [...] quantum integrability is implied by the existence of (countable) infinite many *local* conserved quantities"). Furthermore it is not clear at all what the degrees of freedom exactly are.

2. To fix the problem from 1. one can define relevant and irrelevant constants of motion. Those constants are supposed to be relevant which in the classical limit have an associated classical constant. This definition does not hold as well because classical limits are not always distinct and not every system can be given a classical limit.

3. Quantum Integrability can also be defined through scattering. If the outgoing scattered state is non-diffractive the system is called integrable. The problem is obviously that this definition is depending on properties of a wave function and thus not really general.

4. Systems are quantum integrable if they can be solved with the Bethe Ansatz. It is suggestive that a definition which is introduced by a solution attempt cannot be general and one for sure would like to have a general definition.

5. Poissonian energy level statistics can be used for the definition of quantum integrability but again this definition is not general.

6. Another non-general definition would be to define quantum integrability through energy level crossings.

7. Exactly solvable quantum systems are integrable.

The result of this list is that the topic of quantum integrability still needs to be investigated more closely. Definition seven seems to be suited as it is general and there are no problems regarding consistency but philosophically one could argue that this definition is just of technical meaning and does not contain any real physical meaning. Fortunately this problem will not show up with the quench investigated later in this thesis for the dynamics can be described quasi classically in most aspects and thus we will rely on definition 1.

1.5.3 Integrability vs. Thermalization

The connection between integrability and thermalization has gained lots of interest in the past ten years since Kinoshita et al. conducted an experiment where a nearly integrable system, known as the Newton's cradle, did not tend to thermalize.[12] They prepared a bose gas such that two groups of atoms with opposite initial momenta were formed which afterwards oscillated in a strict one-dimensional tube and could scatter with each other. They showed that even weak non-integrable elements apparently do not lead to thermalization on the time scale tracked by the experiment.

In general it is assumed that integrability prevents thermalization. Regarding classical mechanics integrability restricts trajectories to a smaller area in phase space due to various conserved quantities and hence the system cannot be ergodic any longer. For that reason classical integrability and thermalization legitimately are intimately interconnected. However, the difficulty of defining quantum integrability opens this topic in terms of quantum mechanics for intense research.

In [11] the driven Rabi model was investigated and it was shown that it would widely be rated as non-quantum integrable. As a result Larson found out that this model does not thermalize despite its non-integrability. Following this result the question if non-integrability and thermalization go hand in hand should be raised.

In this thesis it will be investigated how two different quantities of the one-dimensional Bose-Hubbard model behave temporally after a quantum quench while the system approaches an integrable point, realized by bringing the masses of two quasi-particle species closer to each other.

1.6 The Bose-Hubbard Model

The Bose-Hubbard model is an approximating theoretical second quantized model for bosonic interactions in lattices. The Hamiltonian for a one-dimensional lattice with L sites is given by

$$\mathcal{H} = -J \sum_{i=1}^{L/L-1} (\hat{a}_{i+1}^{\dagger}\hat{a}_i + \hat{a}_i^{\dagger}\hat{a}_{i+1}) + \frac{U}{2}\sum_{i=1}^{L}\hat{n}_i(\hat{n}_i - 1) - \mu\sum_{i=1}^{L}\hat{n}_i \tag{1.30}$$

with the bosonic creation and annihilation operators $\hat{a}_i$ and $\hat{a}_i^{\dagger}$ operating on site i as well as the occupation number operator $\hat{n}_i$ for site i and the sums run over all sites. The upper bound of the first sum depends on the boundary conditions. For fixed boundary conditions (i.e. the particles are arranged in a linear array and at the ends there are non-interacting walls) the sum runs to $L-1$ because in this case $\hat{a}_{L+1}$ has no meaning. The other possible boundary condition (i.e. the particles are arranged in a circle where the $(L+1)^{\text{th}}$ site is associated with the first site) is a periodic one where the sum runs to L. μ in the third term is referred to as the chemical potential which is used for a grand-canonical description. J is a measure for the energy gained when particles hop from one site to another, thus it is often referred to as hopping energy or in some sense hopping rate (but with caution as it has the dimension of energy). It can be manipulated experimentally by adjusting the dipole potential's height (see fig.3). U describes the repulsive interaction between particles on one site. In more than one dimension the sum in the first term runs over all neighbors $\langle i, j\rangle$.

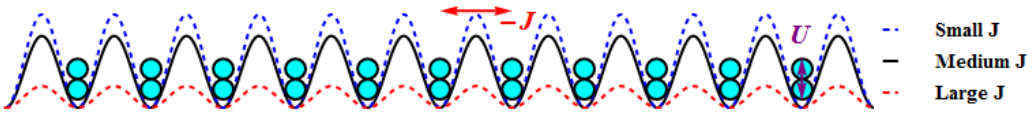

Figure 3: *Schematic image of a bose gas in a one-dimensional optical lattice described by the Bose-Hubbard Hamiltonian. The periodic potential is plotted for three different magnitudes of the hopping rate J. As the potential increases J decreases.*

As there is equivalence between the dimension of the Hilbert space $\mathfrak{H}$ of a one-dimensional lattice with size L and particle number n and the number of possibilities of choosing n not necessarily different elements from a set with L different elements with disregard to the order a combinatorical calculation provides us with the dimension

$$\dim \mathfrak{H} = \binom{L+n-1}{n} \quad . \tag{1.31}$$

Neglecting the third term the model effectively contains just one parameter J/U (or U/J) as

one can measure energies in units of J or U

$$\mathcal{H}_J = \left(-\sum_{i=1}^{L} (\hat{a}_i \hat{a}_{i+1}^\dagger + \hat{a}_i^\dagger \hat{a}_{i+1}) + \frac{U}{2J} \sum_{i=1}^{L} \hat{n}_i(\hat{n}_i - 1) \right) J$$
$$\mathcal{H}_U = \left(-\frac{J}{U} \sum_{i=1}^{L} (\hat{a}_i \hat{a}_{i+1}^\dagger + \hat{a}_i^\dagger \hat{a}_{i+1}) + \frac{1}{2} \sum_{i=1}^{L} \hat{n}_i(\hat{n}_i - 1) \right) U \quad . \tag{1.32}$$

There are two limiting cases:

1. $J/U \ll 1$: Mott insulator—characterized by strong coupling and weak hopping rate.
2. $J/U \gg 1$: Super-fluid phase—characterized by weak coupling and extensive hopping.

Both limits are worth to be investigated. Albeit this thesis will merely deal with case one.

The derivation of the Bose-Hubbard Hamiltonian uses Bloch- as well as Wannier-States and assumes small overlap of neighboring wave functions. It will not be done here, for a complete derivation see for example [13].

2 Weak Quantum Quench in the one-dimensional Bose-Hubbard Model

2.1 Introduction

We want to study a weak quantum quench in the one-dimensional Bose-Hubbard model with energy conservation and momentum conservation modulo 2π where we start with $U \gg 1$, $J = 0$ and then set J up to an finite value with $J/U \ll 1$ (or equivalently do a quench from $U = \infty$ to a finite U with $J/U \ll 1$). Let us exclude the chemical potential so that in (1.30) the third term vanishes. The lattice constant will be set to $a = 1$ so that the spatial position of the sites can be associated with integers from 1 to L. We use fixed boundary conditions but as in our simulation later on the lattice length will be set to a hugely high magnitude of $\mathcal{O}(10^8)$ the boundary conditions will not effect our results. The quench equation then reads

$$\begin{aligned} t < 0: \quad & \mathcal{H}_0 = \mathcal{H}_{B-H}(J=0) = \frac{U}{2}\sum_{i=1}^{L} \hat{n}_i(\hat{n}_i - 1) \\ (t = 0^- \to t = 0^+): \quad & \downarrow \\ t \geq 0: \quad & \mathcal{H} = \mathcal{H}_0 - J\sum_{i=1}^{L-1}(\hat{a}_{i+1}^\dagger \hat{a}_i + \hat{a}_i^\dagger \hat{a}_{i+1}) = \mathcal{H}_{B-H}(J \neq 0, J/U \ll 1) \quad . \end{aligned} \tag{2.1}$$

Let the number of particles be $n = N \cdot L$ with an for now unspecified integer N. For J is equal to zero and U attains an infinitely high value all sites will be equally occupied by N particles at $t < 0$ due to minimization of potential energy given by eigenvalues of $\mathcal{H}_0$. Other configurations are suppressed due to the large value of U. Directly after the quench the only thing that can happen is the formation of quasi particles by hopping of real particles. Since J/U is very small excitations with less than $N-1$ or more than $N+1$ particles per site have a very low probability and will be ignored furthermore. This gives us two species of excitations or quasi-particles, those with $N+1$ particles per site and those with $N-1$. We first want to investigate the properties of these excitations, namely properties of the starting configuration ($t = 0^+$), the momentum distribution and the excitation energy. Hereof mainly the kinetic energy (given by the J-term) will be of interest for the simple reason that for a given number (which will be determined by a certain probability and weakly fluctuate around an expectation value) of quasi-particles the potential energy (U-term) is constant all the time.

2.2 Properties at $t = 0^+$

2.2.1 Formation of quasi-particles

For comfortability the excitation with $(N-1)$ particles per site will be furthermore referred to as "heavyon" and the one with $(N+1)$ particles per site as "lighton". The reason for this

naming will become clearer in chapter 3. For $N = 1$ they are known as "doublons" (for lightons) and "holons" (for heavyons).[2]

We first consider a single heavyon-lighton excitation at $t = 0^+$. As there are at all only three different occupation numbers one can easily replace the description via occupation numbers by the description via positions

$$|x_h, x_l\rangle := |N, \ldots, \underbrace{N+1}_{(x_l)^{\text{th}}\text{ site}}, \ldots, \underbrace{N-1}_{(x_h)^{\text{th}}\text{ site}}, \ldots, N\rangle \quad , \quad x_h \neq x_l \tag{2.2}$$

and momenta $|q_h, q_l\rangle$. If we define the above mentioned state at $t = 0^-$ as $|N\rangle = |N, \ldots, N\rangle$ then

$$\{|N\rangle, \{|x_h, x_l\rangle\}_{x_h, x_l = 1,2,\ldots,L, x_h \neq x_l}\}$$

span the space of possible states at $t = 0$. These basis states can be chosen orthonormal for tunneling is suppressed by $(J/U)^2$ ([2]) and thereby will be neglected. Introducing centre-of-mass coordinates simplifies the following work, so we define

$$\begin{aligned} X &:= \frac{x_h + x_l}{2} \quad , \quad x := x_h - x_l \\ K &:= q_h + q_l \quad , \quad q := \frac{q_h - q_l}{2} \quad . \end{aligned} \tag{2.3}$$

By making use of discrete Fourier transform one can switch between spatial representation and representation by momentum:

$$\begin{aligned} \left\{ |K, .\rangle = \frac{1}{\sqrt{L}} \sum_X e^{iKX} |X, .\rangle \ , \ |., q\rangle = \frac{1}{\sqrt{L}} \sum_x e^{iqx} |., x\rangle \right\} \\ \Rightarrow |K, q\rangle = \frac{1}{L} \sum_X \sum_x e^{i(KX+qx)} |X, x\rangle \quad . \end{aligned} \tag{2.4}$$

In fact $|., q\rangle$ has to be written as $\frac{1}{\sqrt{L}}|., q\rangle = \sum_x \sin(q|x|)|., x\rangle$ since $|., x = 0\rangle$ can not contribute to $|., q\rangle$ as it is equivalent to $|N\rangle$. When calculating the kinetic energies later on we will mix up sin and e to keep the calculation as simple as possible. Nevertheless the results will be the same as by using sin permanently.
Applying the new Hamilton operator $\mathcal{H}$ on $|N\rangle$ and using $|X, x\rangle$ yields to

$$\begin{aligned} \mathcal{H}|N\rangle &= \mathrm{c}|N\rangle - J \left(\sum_i \hat{a}_{i+1}^\dagger \hat{a}_i + \hat{a}_i^\dagger \hat{a}_{i+1} \right) |N\rangle \\ &= \mathrm{c}|N\rangle - d \sum_X \left(|X, 1\rangle + |X, -1\rangle \right) \\ &= \mathrm{c}|N\rangle - d \sum_X e^{iX \cdot 0} \left(|X, 1\rangle + |X, -1\rangle \right) \\ &\overset{\text{FT}}{=} \mathrm{c}|N\rangle - d \left(|K = 0, 1\rangle + |K = 0, -1\rangle \right) \end{aligned}$$

with constants c and d that are not of interest for now. Using the previous calculation the transition rate becomes

$$\begin{aligned}\langle K,x|\mathcal{H}|N\rangle &\overset{\text{ortho}}{=} c\underbrace{\langle K,x|N\rangle}_{=0} - d\left(\langle K,x|K=0,1\rangle + \langle K,x|K=0,-1\rangle\right)\\ &= -d(\delta_{K,0}\delta_{x,1}\||0,1\rangle\|^2 + \delta_{K,0}\delta_{x,-1}\||0,-1\rangle\|^2)\\ &= -d\delta_{K,0}\delta_{|x|,1}(\||0,1\rangle\|^2 + \||0,-1\rangle\|^2) \quad .\end{aligned}$$

This means

$$\langle K,x|\mathcal{H}|N\rangle \sim \delta_{K,0}\delta_{|x|,1} \quad , \tag{2.5}$$

thus heavyon-lighton pairs always arise at neighbored sites with total momentum $K = 0$ and therefore with opposite single momenta

$$\begin{aligned}x_h &= x_l \pm 1\\ q_h &= -q_l \quad .\end{aligned} \tag{2.6}$$

2.2.2 Kinetic Energy

The observed quench uses $J/U \ll 1$ and regarding eq.(1.32) it seems to be opportune to use J/U as a small perturbation parameter to calculate the kinetic energies of heavyons and lightons through perturbation theory of first order in J/U

$$\begin{aligned}&\tilde{\mathcal{H}}_0 \longrightarrow \tilde{\mathcal{H}} = \tilde{\mathcal{H}}_0 - \lambda\tilde{\mathcal{H}}_1 \quad , \quad \lambda = (J/U)\\ &\tilde{\mathcal{H}}_0 := \frac{1}{U}\mathcal{H}_0 \quad , \quad \tilde{\mathcal{H}}_1 := \sum_i \hat{a}_{i+1}^\dagger\hat{a}_i + \hat{a}_i^\dagger\hat{a}_{i+1} \quad .\end{aligned} \tag{2.7}$$

As we factored out U here it has to been multiplicated with the results later.
Fortunately we have already calculated that $K = 0$ and so the most suited representation to work with is $|K,q\rangle$ with $K = 0$. The first ordered energies can be calculated as

$$\begin{aligned}E_N^{(1)} &= -\lambda U\langle N|\underbrace{\tilde{\mathcal{H}}_1|N\rangle}_{\neq a|N\rangle} \overset{ortho}{=} 0\\ E_q^{(1)} &= -\lambda U\langle 0,q|\tilde{\mathcal{H}}_1|0,q\rangle = E_{kin,hl}\\ E_{tot,hl} &= E_{pot,hl} + E_{kin,hl} \quad .\end{aligned}$$

To calculate $E_q^{(1)}$ we apply $\tilde{\mathcal{H}}_1$ on $|0,q\rangle$

$$\begin{aligned}
\tilde{\mathcal{H}}_1|0,q\rangle &= \tilde{\mathcal{H}}_1\left(\frac{1}{L}\sum_X\sum_x e^{iqx}|X,x\rangle\right)\\
&\overset{(*)}{=} \frac{1}{L}\Bigg(\sum_X\sum_x e^{iqx}\Big(N\left(\Big|X+1/2,x+1\Big\rangle+\Big|X-1/2,x-1\Big\rangle\right)\\
&\quad+(N+1)\left(\Big|X+1/2,x-1\Big\rangle+\Big|X-1/2,x+1\Big\rangle\right)\Big)\Bigg)\\
&\quad+\frac{1}{L}\sum_X\sqrt{N(N+1)}\Big(\sin(q|1|)+\sin(q|-1|)\Big)|N\rangle\\
&\overset{(**)}{\approx} \frac{2}{L}\left(\sum_X\sum_{\tilde{x}} e^{iq\tilde{x}}\Big(N\cos(q)+(N+1)\cos(q)|X,\tilde{x}\rangle\Big)\right)+2\sqrt{N(N+1)}\sin(q)|N\rangle\\
&= 2(N+(N+1))\cos(q)|0,q\rangle+2\sqrt{N(N+1)}\sin(q)|N\rangle
\end{aligned}$$

For the understanding of step $(*)$ it is useful to consider fig.4. The first four summands in the first term are displayed and one can see which prefactors $\hat{a}_i\hat{a}_i^\dagger$ produces in each of those cases. Recombination leads to the second term. In the first term the exponential representation of $|.,q\rangle$ was used for simplicity in the second it was necessary to use sine. Step $(*)$ uses the transformations $x\mapsto\tilde{x}=x\pm1$ as well as $\cos(q)=\frac{1}{2}\left(e^{iq}+e^{-iq}\right)$ and $\sum_X\left|X+1/2,x\right\rangle\approx\sum_X\left|X-1/2,x\right\rangle\approx\sum_X|X,x\rangle$ for large L.

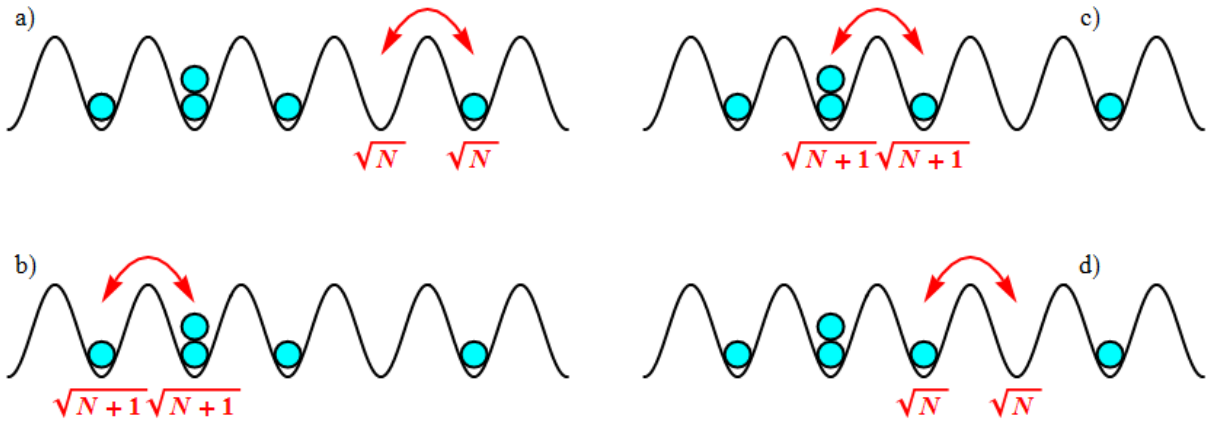

Figure 4: *There are five possible ways* $\tilde{\mathcal{H}}_1$ *can act on a heavyon-lighton excitation, four are shown for* $N=1$ *and the fifth is recombination with gives a factor* $\sqrt{N(N+1)}$ *:*

a) $X\mapsto X+\frac{1}{2}$, $x\mapsto x+1$, *c)* $X\mapsto X+\frac{1}{2}$, $x\mapsto x-1$
b) $X\mapsto X-\frac{1}{2}$, $x\mapsto x+1$, *d)* $X\mapsto X-\frac{1}{2}$, $x\mapsto x-1$

As the previous calculation has shown the total kinetic energy of a heavyon-lighton excitation is

$$E(q) = E_{kin,hl} \approx -2J(N + (N+1))\cos(q) \quad . \tag{2.8}$$

Heavyons contribute to hopping with N and lightons with $N+1$, thus the single energies are

$$\epsilon_h(q) \approx -2NJ\cos(q) \quad , \quad \epsilon_l(q) \approx -2(N+1)J\cos(q) \quad . \tag{2.9}$$

where $K = 0$ results in $q = \pm q_{l/h}$. Velocities are given by the energy derivatives $v = \frac{\partial \epsilon}{\partial q} \sim +\sin(q)$.

2.2.3 Quasi-Particle Density

Denoting the initial state directly after the quench with $|\Psi\rangle_{ini}$ the the quasi-particle density in dependency of q at $t = 0^+$ is given by

$$n_q(0^+) = |\langle 0, q|\Psi\rangle_{ini}|^2 \quad .$$

Following perturbation theory $|\Psi\rangle_{ini}$ is calculated in first order as

$$|\Psi\rangle_{ini} = |N\rangle^{(0)} - \lambda\left(|\tilde{N}\rangle^{(1)} + |0, \tilde{q}\rangle^{(1)}\right) \cdot U$$

with

$$|\tilde{N}\rangle^{(1)} = \sum_q |0, q\rangle^{(0)} \frac{{}^{(0)}\langle 0, q|\tilde{\mathcal{H}}_1|N\rangle^{(0)}}{E_N^{(0)} - E_q^{(0)}}$$

$$|0, \tilde{q}\rangle^{(1)} = \sum_{q' \neq q} |0, q'\rangle^{(0)} \underbrace{\frac{{}^{(0)}\langle 0, q'|\tilde{\mathcal{H}}_1|0, q\rangle^{(0)}}{E_q^{(0)} - E_{q'}^{(0)}}}_{=0} + |N\rangle^{(0)} \frac{{}^{(0)}\langle N|\tilde{\mathcal{H}}_1|0, q\rangle^{(0)}}{E_q^{(0)} - E_0^{(0)}}$$

where

$$E_N^{(0)} = \frac{U}{2} LN(N-1)$$

$$E_q^{(0)} = \frac{U}{2}\left((L-2)N(N-1) + (N+1)N + (N-1)(N-2)\right) = E_N^{(0)} - U$$

and ${}^{(0)}\langle 0, q|\tilde{\mathcal{H}}_1|$ has already been calculated. The final result for $|\psi\rangle_{ini}$ eventually is

$$|\Psi\rangle_{ini} = \left(1 - \frac{2J\sqrt{N(N+1)}}{U}\sin(q)\right)|N\rangle - \frac{2J\sqrt{N(N+1)}}{U}\sum_q \sin(q)|0, q\rangle$$

and thus one obtains the particle distribution

$$n_q(0^+) = \frac{4(N+1)NJ^2}{U^2}\sin^2(q) \quad . \tag{2.10}$$

From this one both the momentum distribution and the mean quasi-particle density can be extracted

$$\begin{aligned} n(0^+) \overset{\text{conserved}}{=} n = \frac{2(N+1)NJ^2}{U^2} \\ p(q) \sim \sin^2(q) \quad . \end{aligned} \tag{2.11}$$

2.3 Hydrodynamics (Theoretical Long-Time Behavior)

The long-time behavior of energy correlations after the mentioned quench can be described by hydrodynamic long-time tails. After a quench the pattern of energy fluctuation changes and afterwards energy has to be transported over large distances in order to build up the equilibrium pattern of fluctuations and by association built up global equilibrium . As energy is conserved the relaxation proceeds very slowly, i.e. $\sim t^{-\frac{1}{2}}$ for long times and not $\sim e^{-t}$ as predicted by Boltzmann equation. The aim of this section is to reproduce the analytic result from [2]. The calculation will be restricted to the relevant one-dimensional case which spares us the notation of vectors.
A conserved quantity can often be described by a continuity equation which is well known e.g. from classical electrodynamics where the continuity equation regarding charge is a cornerstone of the theory. Thus energy conversation is described by

$$\partial_t e + \partial_x j_e = 0 \tag{2.12}$$

with the energy density e , $[e] = \frac{E}{L}$ and the energy current density j_e. In approximation one can express j_e as

$$j_e = -D(\omega, N)_e \partial_x e - f$$

where f , $[f] = \frac{E}{LT}$ denotes a noise term caused by thermal fluctuations and $D(\omega)_e$, , $[D] = \frac{L^2}{T}$ a diffusion constant depending on frequency and N from the previous sections, i.e. particles per site. The purpose lies on observations of long times and thus $\omega \approx 0$, so the notation will be $D(0, N)_e \equiv D_e$ as the N-dependency is not relevant with regard to the following calculations. Inserting it into (2.12) yields to the diffusion equation

$$\partial_t e - D_e \partial_x^2 e = \partial_x f \quad . \tag{2.13}$$

Solving this equation requires the Green's function G which satisfies

$$\partial_t G(x, x', t, t') - D_e \partial_x^2 G(x, x', t, t') = \delta(x - x')\delta(t - t') \quad . \tag{2.14}$$

Translational invariance of (2.13) allows to replace $G(x, x', t, t') \mapsto G(x - x', t - t')$. By setting $x' = 0$, $t' = 0$ and mount it at the end will spare a bit of paperwork. If $G(x, t)$ is known the

energy density can be calculated by integrating (noted $e(x,0) = e_0(x)$)

$$e(x,t) = \int_{\mathbb{R}} \mathrm{d}x'\, e_o(\tilde{x}) G(x-x',t) + \int_{\mathbb{R}} \mathrm{d}x' \int_{\mathbb{R}_0^+} \mathrm{d}t'\, G(x-x',t-t')\partial_{x'} f(x',t') \quad . \tag{2.15}$$

Performing a Fourier transform puts itself forward for calculating $G(x,t)$. Hence we write

$$G(x,t) = \frac{1}{(2\pi)^2} \int_{\mathbb{R}} \mathrm{d}k \int_{\mathbb{R}} \mathrm{d}\omega\, e^{iwt} e^{ikx} \hat{G}(k,\omega) \quad .$$

Under a Fourier transform the derivatives behave like $\partial_t \mapsto i\omega$, $\partial_x \mapsto ik$, the delta distribution transforms to $\hat{\delta}_{\omega,k} = \frac{1}{2\pi}$ and thus the transformed Green's function becomes

$$\hat{G}(k,\omega) = \frac{1}{4\pi^2(i\omega + D_e k^2)} \quad .$$

In order to do the back transformation we set $\hat{G}_k(\omega)$ as a function of ω for constant k. Since $\hat{G}_k(\omega)$ has a single pole at $\omega = iD_e k^2$ the residue theorem claims that for $t > 0$

$$\begin{aligned}
G_k(t) &= \int_{\mathbb{R}} \mathrm{d}\omega\, \hat{G}(\omega) e^{i\omega t} = 2\pi i \mathrm{Res}_{iD_e k^2}\left(\hat{G}_k(\omega) e^{i\omega t}\right) \\
\mathrm{Res}_a(f(z)) &= \lim_{z\to a}(z-a) f(z) \\
&\Downarrow \\
G_k(t) &= \frac{2\pi}{4\pi^2} i \underbrace{\lim_{\omega \to iD_e k^2} \frac{\omega - iD_e k^2}{i\omega + D_e k^2}}_{=-i} e^{i\omega t} \\
&= \frac{1}{2\pi} e^{-D_e k^2 t} \quad , \quad t > 0 \\
&= \frac{1}{2\pi} e^{-D_e k^2 t} \Theta(t)
\end{aligned}$$

Using the well-known Gaussian formula $\int_{\mathbb{R}} \mathrm{d}x\, e^{-ax^2+bx} = \sqrt{\frac{\pi}{a}} e^{\frac{b^2}{4a}}$ one can easily calculate the fully back-transformed Green's function

$$\begin{aligned}
G(x,t) &= \int_{\mathbb{R}} \mathrm{d}k\, \underbrace{G(k,t)}_{G_k(t)} e^{+ikx} \\
&= \frac{e^{-x^2/(4D_e t)}}{\sqrt{4\pi D_e t}} \Theta(t) \quad .
\end{aligned} \tag{2.16}$$

Using (2.15) and assuming $\langle e_0(x)\partial_{x'} f(x',t)\rangle = 0$ the energy correlation at time t reads

$$\begin{aligned}\langle e(x,t)e(x',t)\rangle = &\int_{\mathbb{R}} \mathrm{d}x_1 \int_{\mathbb{R}} \mathrm{d}x_2\, G(x-x_1,t)G(x'-x_2,t)\langle e_0(x)e_0(x')\rangle \\ &+ \int_{\mathbb{R}_0^+} \mathrm{d}t_1 \int_{\mathbb{R}_0^+} \mathrm{d}t_2 \int_{\mathbb{R}} \mathrm{d}x_1 \int_{\mathbb{R}} \mathrm{d}x_2 \Big[G(x-x_1,t-t_1)G(x'-x_2,t-t_2) \\ &\langle \partial_{x_1} f(x_1,t_1)\partial_{x_2} f(x_2,t_2)\rangle\Big]\end{aligned} \tag{2.17}$$

The form of the noise correlation is derived by the well-known thermodynamical expression for the energy fluctuation $(\langle e^2\rangle - \langle e\rangle^2)_{eq} = c_V k_B T^2$, achieved by a grand-canonical calculation which is usually done within a standard statistical physics lecture, with the specific heat c_V. The effective temperature of the equilibrium state after the observed quench is $T = \infty$ because , as we will see in later in chapter 3, the momentum distribution flattens and for $t \to \infty$ all momenta are equally probable. Thermodynamical this means $e^{-\frac{\epsilon(q)}{k_B T}} = 1$ and thus $T = \infty$. Since $\langle e_0\rangle = \int \mathrm{d}q\, p_0(q)e(q) = 0 \overset{\text{energy conservation}}{=} \langle e(t)\rangle \ \forall t > 0$ the spatial energy correlations can approximately be expressed by

$$\langle e(x)e(x')\rangle_{eq} = c_V k_B T^2 \delta(x-x') \tag{2.18}$$

where the approximation concerns the locality. Although the temperature is infinite, the equilibrium energy correlation is finite due to the fact that the heat capacity vanishes and the product takes on a finite value. As hydrodynamics describe systems well for long time and length scales this approximation will be sufficient in order to achieve suiting results. The spatial and temporal correlation of a noise term should be zero since consecutive statistical fluctuations should be widely independent. Eventually one approximates $\langle f(x,t)f(x',t')\rangle = A\delta(x-x')\delta(t-t')$. The prefactor A can partly be guessed by dimensional treatment or calculated using Fourier transform, eq.(2.18) and eq.(2.17). It was done by [2] and the result is

$$\langle f(x,t)f(x',t')\rangle = 2k_B T^2 c_V D_e \delta(x-x')\delta(t-t') \quad . \tag{2.19}$$

With this result and $G(x=\infty,t) = G(x=-\infty,t) = 0 \ \forall t > 0$ one can do a partial integration of the second term in (2.17) three times (first two times to translate the derivatives from the deltas to the Green's functions) without receiving boundary terms and by making advantage of the delta distributions property one gets for the second term

$$\begin{aligned}&2k_b c_V T^2 D_e \int_{\mathbb{R}_{\not<}^+} \mathrm{d}t_1 \int_{\mathbb{R}} \mathrm{d}x_1 \Big(\partial_{x_1} G(x-x_1,t-t_1)\Big)\Big(\partial_{x_1} G(x'-x_1,t-t_1)\Big) \\ =& -2k_B c_V T^2 D_e \int_{\mathbb{R}_{\not<}^+} \mathrm{d}t_1 \int_{\mathbb{R}} \mathrm{d}x_1\, G(x-x_1,t-t_1)\Big(\partial_{x_1}^2 G(x'-x_1,t-t_1)\Big) \quad .\end{aligned}$$

The partial integration from the first to the second step can be also be done otherwise such that the term becomes

$$-2k_B c_V T^2 D_e \int_{\mathbb{R}^+_\nu} \mathrm{d}t_1 \int_{\mathbb{R}} \mathrm{d}x_1 \left(\partial^2_{x_1} G(x-x_1,t-t_1)\right) G(x'-x_1,t-t_1) \quad .$$

Thus one can sum up both results and divide by 2 and receives :

$$\begin{aligned} &- k_B c_V T^2 D_e \int_{\mathbb{R}^+_\nu} \mathrm{d}t_1 \int_{\mathbb{R}} \mathrm{d}x_1 \Big[G(x-x_1,t-t_1)\Big(\partial^2_{x_1} G(x'-x_1,t-t_1)\Big) \\ &+ \Big(\partial^2_{x_1} G(x-x_1,t-t_1)\Big) G(x'-x_1,t-t_1)\Big] \quad . \end{aligned}$$

Reorganizing of eq.(2.14) provides an expression for $\partial^2_x G$

$$\partial^2_{x_1} G(x-x_1,t-t_1) = \frac{1}{D_e}\Big(\partial_t G(x-x_1,t-t_1) - \delta(r-r_1)\delta(t-t_1)\Big) \quad .$$

Inserting this into the above term, using $G(x-x_1,t-t_1)\partial_t G(x'-x_1,t-t_1) + G(x'-x_1,t-t_1)\partial_t G(x-x_1,t-t_1) = \partial_t\Big(G(x-x_1,t-t_1)G(x'-x_1,t-t_1)\Big)$, $G(x-x_1,0) = \frac{1}{2}\delta(x-x_1)$ (as it is half a Dirac's sequence), $G(.,-\infty)=0$ and $\int_{\mathbb{R}} \mathrm{d}x_1\, \delta(x-x_1)\delta(x'-x_1) = \delta(x-x')$, one receives

$$\begin{aligned} & k_B c_V T^2 \Big(- \int_{\mathbb{R}} \mathrm{d}x_1\, G(x-x_1,t) G(x'-x_1,t) + \delta(x-x')\Big) \\ \overset{(2.18)}{=} & - \int_{\mathbb{R}} \mathrm{d}x_1 \int_{\mathbb{R}} \mathrm{d}x_2 \left(G(x-x_1,t) G'(x-x_2,t) \langle e(x_1)e(x_2)\rangle_{eq}\right) + \langle e(x)e(x')\rangle_{eq} \quad . \end{aligned}$$

Now the first term of (2.17) can be added to this result to achieve an expression for the deviation of the energy correlation at time t from the equilibrium correlation

$$\begin{aligned} \langle e(x,t)e(x',t)\rangle - \langle e(x)e(x')\rangle_{eq} = & \\ \int_{\mathbb{R}} \mathrm{d}x_1 \int_{\mathbb{R}} \mathrm{d}x_2\, G(x-x_1,t) G(x'-x_2,t) \Big[\langle e_0(x_1)e_0(x_2)\rangle - \langle e(x_1)e(x_2)\rangle_{eq}\Big] & \end{aligned}$$

In the investigated system energy correlations at $t = 0^+$ are quite local, in fact the only non vanishing correlation is the next neighbor correlation. Concerning this it is a very good assumption to say $\langle e_0(x)e_0(x')\rangle \sim \delta(x-x')$. One can also easily confirm that $\int_{\mathbb{R}} \mathrm{d}x_1\, G(x-x_1,t)G(x'-x_1,t) = G_{2D_e}(x-x',t)$. Thus the final proportionality is

$$\begin{aligned} \langle e(x,t)e(x',t)\rangle - \langle e(x)e(x')\rangle_{eq} &\sim \frac{1}{\sqrt{D_e t}} e^{\frac{-(x-x')^2}{8D_e t}} \\ &\sim \frac{1}{\sqrt{t}} \quad t\to\infty \quad . \end{aligned} \tag{2.20}$$

One can see that the system approaches equilibrium only algebraically for very long times but still fast enough so that after a certain time the deviation numerically fluctuates around zero. In an arbitrary dimension d the proportionality is $\sim t^{-d/2}$ which is an effect of the Gaussian integral

when calculating $G(x,t)$. The dimension does not make a difference in the rest of the calculation.

2.4 Numerical Method

Sachdev and Young introduced a semi-classical approach for relaxational dynamics in one-dimensional quantum systems.[1] It has been applied to quantum quenches in [14] to study finite transverse Ising chains and finite size effects as well as in [2] and [3] for the investigation of the one-dimensional Bose-Hubbard model.
In this case for sufficiently small values of J/U the particles mean distance $\langle d\rangle = \frac{1}{n_0^+} = \frac{U^2}{2N(N+1)J^2}$ is much larger than their thermal De Broglie wavelength $\lambda \sim \sqrt{2mT}^{-1/2}$. The quasi-particle interaction than can be described in a ballistical model where a quasi-particle is associated with a point mass which moves uniformly with velocity $v_{h,l}(q) = \partial_q \epsilon_{h,l}(q)$ after they have been created with opposite momenta obeying the momentum distribution $p_0(q) = \frac{2}{\pi}\sin^2(q)$ where the prefactor takes into account the normalization

$$\int_0^\pi \mathrm{d}q\, p_0(q) = 1 \tag{2.21}$$

as for a pair one has $p_0(q_h) = p_0(q_l)$ and thus the probability of the right quasi-particle to have a momentum between 0 and π must be one because in lattices the momentum is restricted to the first Brillouin zone which in one dimension is $|q| \leq \frac{\pi}{a}$ and we set $a = 1$. Quasi-particles can scatter i.e. collide ballistically if their distance is $d = \Delta t \delta v$. The chance of tunneling will be neglected, indeed in [2] a finite tunnel probability for $N = 1$ was included but did not have an influence on the results. Neither recombination will be considered in this simulation for it is rare. When scattering the particles must obey energy conservation and momentum conservation modulo 2π

$$\left.\begin{aligned} &q_1 + q_2 = q_1' + q_2' + 2i\pi \quad i \in \mathbb{N} \\ &\qquad\qquad\qquad\qquad\qquad\qquad \Big\} \Rightarrow e(q_1) + e(q_2) = e(q_1') + e(q_1 + q_2 - q_1') \\ &e(q_1) + e(q_2) = e(q_1') + e(q_2') \quad . \end{aligned}\right. \tag{2.22}$$

The energy is $\sim cos(q)$ and so the umklapp scattering $2i\pi$ does not influence the energy conservation relation. If two particles of the same species scatter their momenta are just exchanged $q_1' = q_2$, $q_2' = q_1$. In the other case if two different species participate in the scattering event their new momenta can be calculated via

$$\begin{aligned} q_l' &= 2\arctan\left(\frac{N\sin(\frac{q_l}{2}+q_h) - (N+1)\sin(\frac{q_l}{2})}{N\cos(\frac{q_l}{2}+q_h) + (N+1)\cos(\frac{q_l}{2})}\right) \in [-\pi,\pi] \\ q_h' &= (q_h + q_l - q_l') \mod 2\pi \quad . \end{aligned} \tag{2.23}$$

By measuring all times in units of the scattering time, which is the time it takes on average for all particles to scatter ones,

$$t_{scat} = \tau = \frac{\text{simulated time}}{\text{number of quasi-particles * number of scattering events}} \quad .$$

all results are independent of mean density. Therefore the mean density was permanently set to $4(J/U)^2 = 0.0004$ with $J = 1$ and $U = 100$.

Now the program which was used shall be explained. The most information is saved in a vector and a multimap of two different structures. The first structure contains all information about one quasi-particle (i.e index, position, momentum, velocity, time of last scattering event, time next scattering event with left and right particle, species and prefactor or alternatively "mass") and is arranged in a vector organized by the index which means by the lattice site the quasi-particle is situated at. Neglecting tunneling and using fixed boundary conditions guarantees the adherence of this order during the whole simulation. The second structure contains all information about a single scattering event (i.e. time of the event, position where it takes place and indices of the involved quasi-particles) which is arranged in a multimap organized by the time of the event. The multimap takes into account equal times in the frame of a double's precision. The computer time is always set to the first element of the scattering list and is actualized after every scattering event. After two quasi-particles have scattered their new scattering events are sorted into the list and the old scattering event is erased. If there exist scattering events of one of the two quasi-particles, that have scattered with their other neighbor, that are obsolete because the new scattering event has been calculated, those events are searched in an epsilon-environment of the predicted obsolete scattering time in the scattering list via an iterator and erased. The environment is necessary regarding the uncertainty of doubles of about 17 significant digits. At each time step quantities such as the energy correlation can be extracted by accessing the particle list. Since the new momentum calculated via the arctan is per definition restricted to the Brillouin zone and umklapp scattering can only appear for the momentum of the other particle, the arctan has to be used once for heavyon (e.g. if the heavyon is the right particle) and once for lighton (e.g. if the lighton is the left particle) in order to guarantee symmetry and correct behavior.
The creation of quasi-particle pairs is simulated by creating two vector elements with positions = indices = i an $i+1$ with probability $4(J/U)^2$ which is the quasi-particle density and running over i from 1 to $L-1$ where L denotes the lattice's length. For that at every site i a random number between 0 and 1 is created by the MT19937 generator of Makoto Matsumoto and Takuji Nishimura provided by the GNU Scientific Library and compared with the probability. If this number is smaller than the probability the particles are created. With probability $\frac{1}{2}$ a heavyon is created at i with momentum $-q$ and a lighton at $i+1$ with momentum q and vice versa. To receive a momentum distributed according to $p_0(q)$ the inverted function p_0^{-1} is calculated and saved within a file for 1000 equally distanced numbers $\{X\}$ (i.e. values of p) between 0 and 1. Given a random number r the corresponding momentum is calculated by linear interpolation

between the both values of $p_0^{-1}(a)$, $p_0^{-1}(b)$ (which are saved in the file) where $a, b \in \{X\}$ and $a \leq r \leq b$. After the initial state is saved the scattering list is filled for the first time.
It have been used about 10^5 quasi-particles and averaged over 10-1200 runs, depending on the quantity to look at and the value of N. Each run was given an integer, starting with one, that served as the seed for the random number generator. Unfortunately it has to be admitted that the results are not fully reproducible with the old C++-standard although a determined seed was given. It could be undefined behavior that has not been detected since the results are reproducible with the C++0x-standard. Another problem emerging is that if two scattering events really have the same scattering time then a non-involved event with scattering time next to those both is erased without doing it by command (as far as recognized till now but not utterly excluded). It again implies undefined and undetected behavior. It can indeed with great certainty be ensured that it does not effect the results when the problematic runs are taken out.

3 Approach to Integrability

3.1 The Method of Approaching

In this thesis we want to observe the temporal behavior after the quench in a crossing where we approach integrability. To guarantee a smooth approach, comparability of the results and the possibility to do simulations for the exact case of integrability avoiding infinities (anticipatory: The limit is $N \to \infty$. In this case the energies would diverge.) we substitute the prefactors

$$N \mapsto 1 \quad , \quad N+1 \mapsto \frac{N+1}{N} \quad . \tag{3.1}$$

This substitution does not effect the temporal behavior of the observed quantities since all times are measured in units of the scattering time which means effectively in numbers of scattering events. Thus the changed velocities and mean density do not have an influence in this measure. Likewise the calculated new momentum after a scattering of two quasi-particles (2.23) is invariant under this transformation. Only prefactors change which has to be respected in some theoretical calculations.

In order to do the crossing let us first resolve what can be called the masses of the quasi-particles. Considering small momenta first one can Taylor expand the dispersion relation in first order with respect to the made substitution

$$\begin{aligned} \epsilon_h(q) &= -2J\cos(q) \approx -2J(1-\frac{1}{2}q^2) = -2J + Jq^2 \;\hat{=}\; \epsilon_0 + \epsilon_{cl}(q) \\ \epsilon_l(q) &\approx -2J\frac{N+1}{N} + J\frac{(N+1)}{N}q^2 \quad . \end{aligned} \tag{3.2}$$

As the classical kinetic energy is $\frac{q^2}{2m}$ one can associate the effective masses with

$$\begin{aligned} m_h &= \frac{1}{2J} \\ m_l &= \frac{N}{2J(N+1)} \quad . \end{aligned} \tag{3.3}$$

Alternatively one could just derive the dispersion relation twice and receive a momentum dependent effective mass

$$\begin{aligned} m &= \frac{1}{\partial^2 E/\partial q^2} \\ m_h(q) &= \frac{1}{2J\cos(q)} \\ m_l(q) &= \frac{1}{2J\frac{N+1}{N}\cos(q)} \quad . \end{aligned} \tag{3.4}$$

In both cases for constant q and N it is $m_h > m_q$ whereby the reason for the naming of *heavyons* and *lightons* should be clear by now. From now on when the terminus masses is used it will always be meant in the sense of (3.3), i.e. non-q-depending.

The limit to take is $N \to \infty$ such that the masses approach each other. For $N = \infty$ the masses and dispersions are exactly the same. In this case particles just exchange momenta so that the momentum distribution and the overall momentum are conserved. Regarding the overall momentum this is caused by prevented umklapp scattering (no umklapp scattering means no convertion of particle momentum to lattice momentum). Actually there exists an infinite number of conserved quantities, e.g. $Q_n = \sum_q \left(q^n \left(n_q^h + n_q^l\right)\right)\ n \in \mathbb{N}$. This means that the number of constants of motion is infinite and thus clearly exceeds the number of degrees of freedom. That implies the system's integrability. It has to be mentioned that the Bose-Hubbard model is a model for dilute gases and thus by making the integrability approach one leaves the scope of application, at least regarding experimental implementation. Preparing a nearly infinite number of bosons in one lattice site on the one hand is a matter of impossibility and on the other hand should clearly lead to further effects that are not covered by the Bose-Hubbard Model. Indeed it is way easier to consider also the extreme case of same masses which can give some indication of the behavior in between as it is done when studying e.g. phase transitions, too. It should not be withhold that it is nevertheless possible to choose $1 \ll N$. $N = 7$, for example, already shows strong influences of the integrable case.
In the following we will consider two averaged quantities

$$\begin{aligned} \langle e_i e_{i+1} \rangle &\overset{\text{numerics}}{=} \frac{1}{L-1} \sum_{i=1}^{L-1} e_i e_{i+1} \\ \langle \cos(2q) \rangle_{l,h} &\overset{\text{numerics}}{=} \frac{1}{L} \sum_{i=1}^{L} \cos(2q)_{i;l,h} \ . \end{aligned} \tag{3.5}$$

We will see that the next neighbor energy correlation $\langle e_i e_{i+1} \rangle$ tends to reach the thermalized value even faster when approaching integrability. One should not be confused for it is not really a matter of thermalization but a property of the special system. One could say the energy correlation forgets its initial state faster by approaching the masses. The $\langle \cos(2q) \rangle_{l,h}$ is related to the momentum distribution at $t = 0^+$ via $\cos(2q) = 1 - 2\sin^2(q)$ of one quasi-particle species and is a measure for the shape of the momentum distribution. As we will see the momentum distribution flattens when thermalizing which prompts the $\langle \cos(2q) \rangle_{l,h}$ to go to zero. By approaching integrability the decay slows down until there is no decay left.
The next two sections cover a discussion of the thermalizing behavior of those two quantities as well as the thermalization's dependency on the masses. In the last section the quantities are compared for a near-equilibrium state. When observing the long-time tails it is necessary to perform a weighted temporal average on the numerical data because the long time regions of both quantities tend to fluctuate around zero more and more by increasing N and thus without temporal averaging it would be difficult to see if a fit-function fits to the data in a plot. To do

the average an on the respective domain normalized Gaussian function was used. When this averaging is used it will be recorded in the captions that it is used and over how many scattering times the average is taken.

3.2 Energy Correlation - A "Forgetful" Quantity

3.2.1 General Behavior

We first want to take a look at the general temporal behavior of the next neighbor energy correlation's expectation/mean value in this section before considering the case of same masses in 3.2.2 and finally observe the long-time behavior in 3.2.3.
The correlations initial value is

$$\langle e_i e_{i+1}\rangle(0^+) = \frac{1}{2}\underbrace{\int_0^\pi \mathrm{d}q\, \epsilon_l(q)\epsilon_h(q)p_0(q)}_{\text{created pairs}} = \frac{1}{2}\frac{N+1}{N} = \frac{1}{2}\frac{m_h}{m_l} \tag{3.6}$$

where the $\frac{1}{2}$ avoids the doubled counting of each pair. The correlation between particles that were not created together vanishes since $\int_0^\pi \mathrm{d}q_1 \int_{-\pi}^0 \mathrm{d}q_2\, \epsilon_{h,l}(q_1)\epsilon_{h,l}(q_2)p_0(q_1)p_0(q_2) = 0$. In a thermalized state the correlation reaches zero as we will see later (eq.(3.16)). It appears that even in the integrable case the correlation approaches zero. It will be explained in the next section. What we focus on now is the sign change. For finite N the sign of the correlation changes from + to -. This is an effect of the different decay of heavyon and lighton momentum distributions. The momentum distribution flattens temporally until all momenta are equally probable (sec.3.3). The zero (i.e. the change of sign) usually is located at a few scattering times (for low N) and goes to infinity for $N \to \infty$. For small N the initial value is a further factor which influences the time of the sign change (fig.6). In fig.5 the momentum distributions of heavyons and lightons for $N = 1$ and few different small times overlaid with a cosine ($\sim \epsilon$) are shown. The critical time interval is the one from 0 to 1.6τ. The heavyon distribution flattens faster than the lightons distribution. This results in an increased number of heavyon-lighton neighbors $\epsilon_h > 0$ and $\epsilon_l < 0$. This contribution surpasses the contribution of neighbors with same-signed energies and thus the correlation's sign changes and for a small time interval afterwards the absolute value increases again. This stops when the decay of heavyon and lighton distributions take on the same temporal behavior. In fig.5 this can be seen between 1.6τ and 2τ where there is no remarkable difference between both times despite similar flattening of both distributions. Afterwards the temporal behavior is dominated by relaxation.

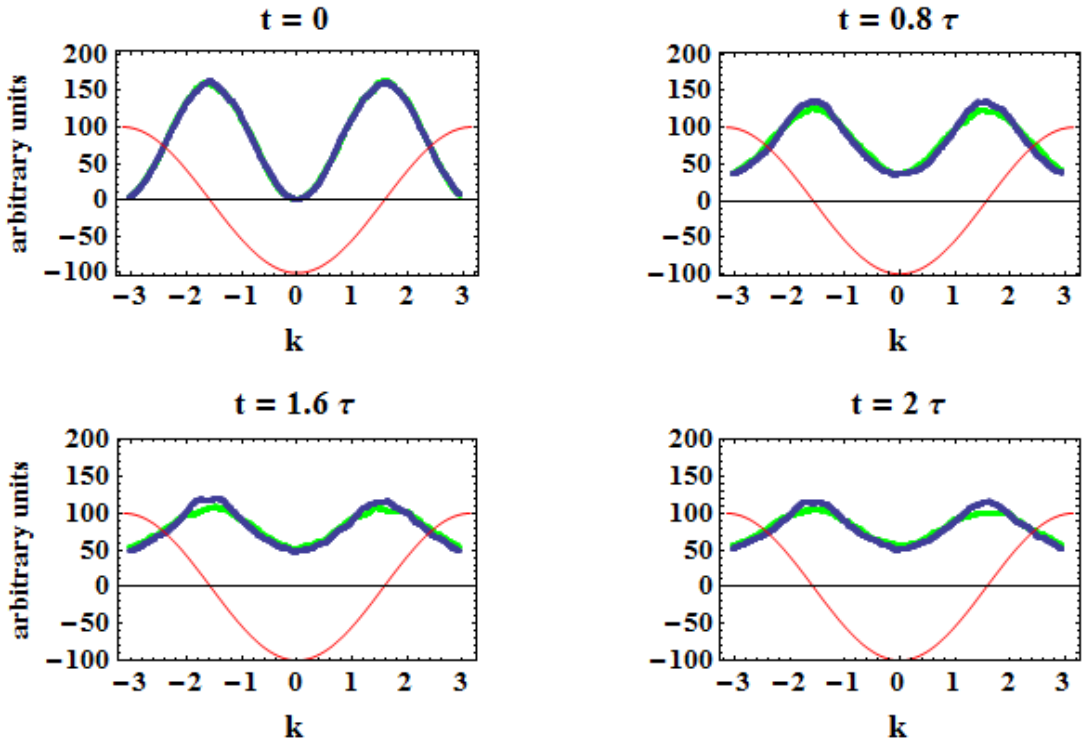

Figure 5: *Momentum distribution of heavyons (green) and lightons (blue) for N=1 and four different small times. It is overlaid with a negative cosine (red) to demonstrate why the sign of the energy correlation changes after few scattering times.*

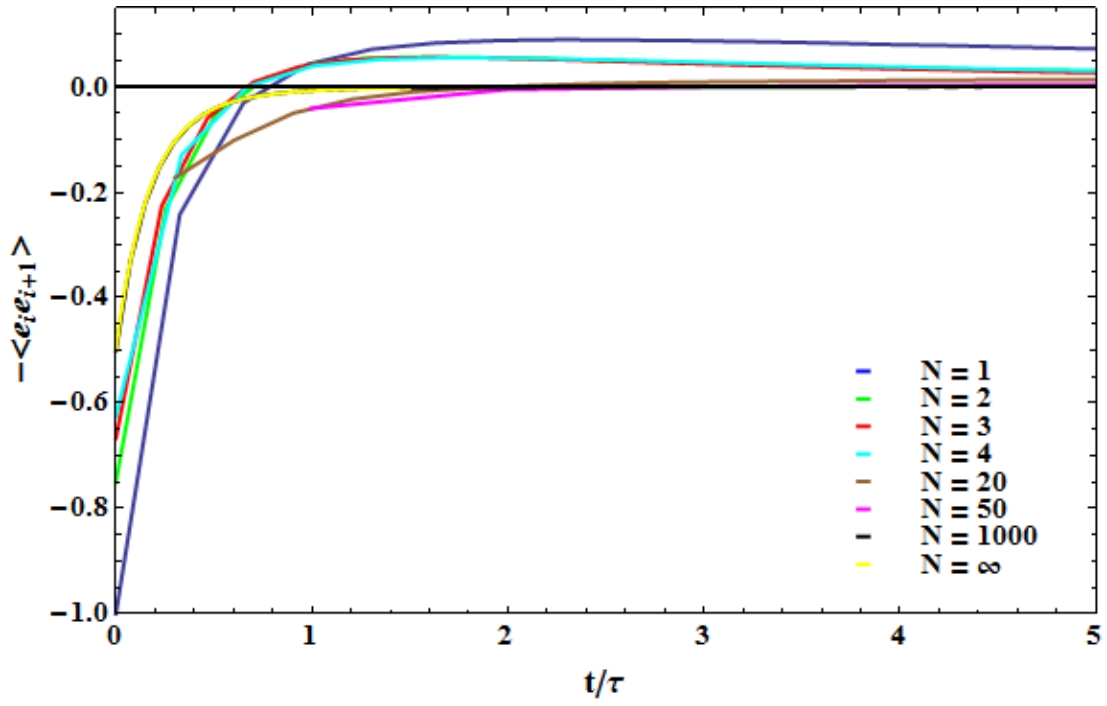

Figure 6: *Energy correlation for various mass ratios and small times. The knees are caused by coarse discretization.*

3.2.2 Same Masses

For small N the short time behavior is dominated by the sign change. It is now interesting how the energy correlation behaves when the particles have the same masses. In order to try to understand it a short calculation can be done and afterwards compared with the numerical result.

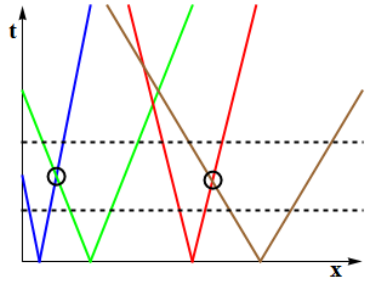

Figure 7: *World lines of quasi-particles for same masses starting at t=0. Quasi-particle are created in pairs with opposite momenta. When quasi-particles scatter momenta are just exchanged and therefore the lines do not show a kink. Correlation of two neighbors are destroyed when different colors are neighbored.*

At $t = 0^+$ the only non-vanishing correlations are on average those of the pairs that have been created together. Normally, if different masses and thus different species are involved, this correlation changes a bit when one of the both particles scatter because the new momentum depends on the old momentum but it is not destroyed. When particles with the same mass are involved the new momentum does not depend on the previous momentum and thus this destroys the correlation of the pair, at least on average. Thus one would expect that the temporal behavior of the overall correlation's expectation value depends on the probability that one particle of a pair has scattered until a time t.
We first need the probability density for a distance d between two neighbored particles that are not in a pair. The probability that a pair is created at sites i and $i+1$ was set to $p = 0.0004$ in the simulation. The distance probability density thus reads

$$p_d(d) = p(1-p)^{d-1} = pe^{d\ln(1-p)} \overset{p\ll 1}{\approx} pe^{-pd}$$

where the finite size of the lattice was neglected which is a good approximation since the simulation uses $L \approx 3 \cdot 10^8$ and $n \approx 10^5$. The probability that the right particle of a pair with momentum $q > 0$ has scattered with its neighbor until time t can further be calculated through

$$\begin{aligned} \mathbb{P}_r(q,t) &= \int_0^t \mathrm{d}\tau \int_{-\pi}^0 \mathrm{d}\tilde{q} \int_0^\infty \mathrm{d}d\, p_0(\tilde{q}) p_d(d) \delta\left(\tau - \frac{d}{\Delta v(q,\tilde{q})}\right) \\ &= \int_0^t \mathrm{d}\tau \int_{-\pi}^0 \mathrm{d}\tilde{q}\, p_0(\tilde{q}) p_d(\tau \Delta v(q,\tilde{q})) \Delta v(q,\tilde{q}) \end{aligned} \tag{3.7}$$

where Δv denotes the difference of velocities $\Delta v = 2(\sin(q) - \sin(\tilde{q})) > 0$ with J set to 1. In

order to scatter at time τ it is necessary that the distance equals $\tau\Delta v$. It is furthermore used that $\delta\left(\frac{x}{a}\right) = |a|\delta(x)$. Actually the integral over τ runs from $\frac{1}{4}$ to t as the distance is restricted to $d \geq a = 1$ and the difference of velocities is restricted to $\Delta v \leq 4$ but it shows that it does not have a noticeable influence on the results.
The energy correlation can also be destroyed when the left particle scatters first. Attributable to symmetry reasons this probability is the same as for the right particle $\mathbb{P}_l = \mathbb{P}_r$. Probability theory tells us that the total probability is expressed by

$$\mathbb{P}_{tot} = \mathbb{P}_(\text{left} \vee \text{right}) = \mathbb{P}_l + \mathbb{P}_r - \mathbb{P}(\text{left} \wedge \text{right}) = 2\mathbb{P}_r - \mathbb{P}_r^2 \quad .$$

Eventually the time-dependent expectation value of the next neighbor energy correlation can be calculated

$$\begin{aligned} \langle e_i e_{i+1}\rangle(t) &= \frac{1}{2}\int_0^\pi \mathrm{d}q \left(1 - \mathbb{P}_{tot}(q,t)\right) p_0(q)\epsilon^2(q) \\ &= \langle e_i e_{i+1}\rangle(0^+) - \frac{1}{2}\int_0^\pi \mathrm{d}q\, \mathbb{P}_{tot}(q,t) p_0(q)\epsilon^2(q) \quad . \end{aligned} \tag{3.8}$$

Nevertheless it can happen that the left particle C_l of the pair C, which is second next in right direction to the considered right particle A_r, scatters with the next pair B, which is situated between A and C, and then the momentum of B_l changes to the momentum of C_l before B_l scatters with A_r. Since all particles are indistinguishable it is equivalent to say that the first scattering of A_r takes place with C_l. It is the same for the left particle and the left direction. So let us consider the influence of second next neighbors (more precisely: particles in second next pairs and with different sign of the momentum) in our calculations. The probability density for the distance between second next neighbors is

$$\begin{aligned} p_{d_2}(d_2) &= \int_0^\infty \mathrm{d}d \int_0^\infty \mathrm{d}d'\, p_d(d) p_d(d') \delta(d_2 - (d + d')) \\ &= \int_0^{d_2} \mathrm{d}d\, p(d) p_d(d_2 - d) \\ &= p^2 d e^{-pd} \quad . \end{aligned}$$

By analogy with (3.7) one can calculate the probability $\mathbb{P}_{r,2}^{\text{pre}}$ that the right particle has scattered with the second next neighbor by time t by replacing p_d with p_{d_2}. We now need the probability that either next or second next neighbors have scattered. Since the events

1. A_r scatters first with B_l

2. A_r scatters first with $C_l \Leftrightarrow A_r$ scatters with C_l and does not scatter with B_l

exclude each other the wanted probability reads

$$\mathbb{P}_{r,2}^{\text{final}} = \mathbb{P}_{r,2}^{\text{pre}} + (1 - \mathbb{P}_r)\mathbb{P}_{r,2}^{\text{pre}} \quad .$$

Similar to the calculation with next neighbor influence the final probability regarding next and second next neighbor influence is

$$\mathbb{P}_{tot,2} = 2\mathbb{P}_{r,2}^{\text{final}} - \left(\mathbb{P}_{r,2}^{\text{final}}\right)^2 \quad .$$

The energy correlation is calculated exactly like in (3.8) using $\mathbb{P}_{tot,2}$ instead of $\mathbb{P}_{tot}$.
Eventually it could be interesting which difference it makes if one works with an averaged energy instead of weighting the probability with the energy such that

$$\langle e_i e_{i+1}\rangle(t) = \langle e_i e_{i+1}\rangle(0^+)\big(1 - \mathbb{P}(t)\big) \quad . \tag{3.9}$$

All mentioned equations have been solved numerically and plotted in units of the scattering time.

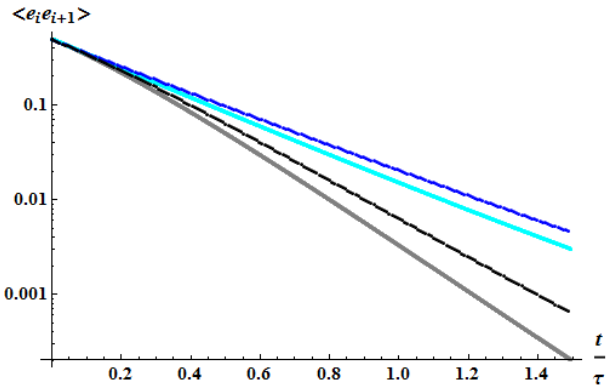

Figure 8: *Comparison of the theoretical results in a log-plot. The curves are: blue - next neighbor influence , cyan - next neighbor influence with averaged energy, black - next and second next neighbor influence, gray - next and second next neighbor influence with averaged energy.*

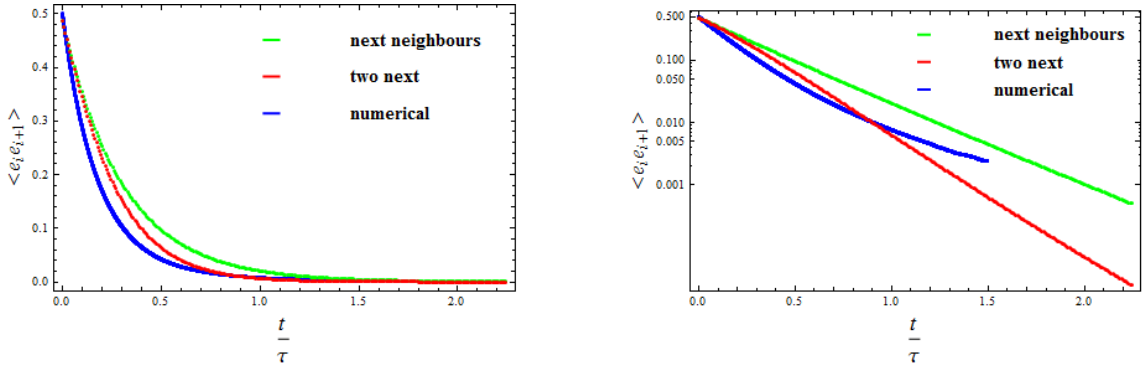

Figure 9: *Comparison of the theoretical curves including both next neighbor influence and next plus second next neighbor influence for the calculation with energy-weighting the probability and the curve received by simulating the system shown in a linear plot (left) and a log-plot (right).*

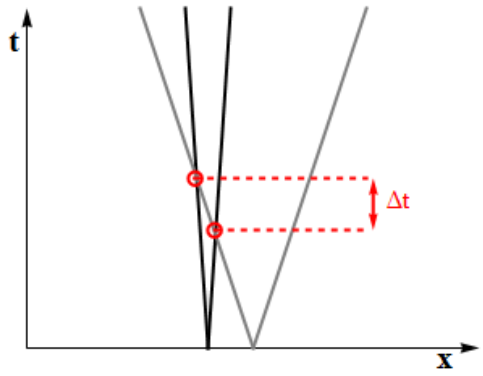

Figure 10: *After a collision neighbors with very low velocities build up their correlation again after a small time*Δt *. It is* $\lim_{v\to 0}(\Delta t)(v) = 0$ *. This is the possible reason for the relaxation of the averaged correlation.*

In fig.8 the theoretical results are compared. One can clearly see that already after a short time next neighbors contribute to the decay in a way such that they cannot be ignored. Using an averaged energy the decay is a little faster than by weighting the probability. This shows up because by proceeding in time the velocity of particles that have not scattered by then becomes smaller. Admittedly the energy increases when the velocity decreases and thus contributes more to the decay but small velocities in turn are very rare. That means that the number of particles that have not scattered decreases very fast. It seems that the effect of decreasing number of left particles exceeds the effect of a higher contribution by their energy resulting in the faster decay by averaging the energy.
In fig.9 the theoretical results are compared to the result received by the simulation. One notices bewilderingly that the simulated energy correlation does not decay exponentially, at least after a very small time a considerable proportion of the exponential decay decreases. One could argue that there is a statistical chance that correlations are built up again but this effect should average to zero. However for particles with $v \sim 0$ the correlation is only destroyed for a very short time Δt after a collision and then built up again (see fig.10). It could be assumed that this effect leads to a relaxation of the averaged correlation's decay. Long-time tails should not contribute to the temporal behavior for they describe thermalization which is excluded in an integrable system. Finally one can say that the calculation which has been made is not sufficient to explain the behavior but provides an approximate description and leastwise explains why the correlation approaches zero although the momentum distribution does not change all the time.

3.2.3 Long-Time Tails

In the following we consider the long-time behavior which is theoretically given by eq.(2.20). It appears that by increasing N (respectively decreasing the mass ratio) the coefficient of the power-law decreases at such a rate and the decay for lower times occurs faster than expected, so that, with respect to the statistical fluctuations of the simulation, the correlation tends to

fluctuate around zero very soon. Therefore it has been possible to extract power laws only for $N = 1, 2, 3$ and only with deployment of temporal averaging.
In fig.12 the received data is plotted in log-log plots and fitted in two different regions. Let us first take a view on the region with $t > 200\tau$. In this long-time region long-time tails as calculated in eq.(2.20) are pronounced. In [2] it has been shown that subleading corrections of $t^{-3/4}$ have to be included using a scaling reflection which takes into account a certain scaling invariance of the diffusion equation. Minding corrections to the energy current like $\alpha\partial_x(e\partial xe)$, $\alpha'\partial_x(n\partial_x e)$ and $\beta\partial_x^4 e$ leads to corrections

$$\langle e(x,t)e(x',t)\rangle - \langle e(x)e(x')\rangle_{eq} \sim \frac{1}{\sqrt{t}} f\left(\frac{x}{\sqrt{t}}, 1, \frac{\alpha}{t^{1/4}}, \frac{\alpha'}{t^{1/4}}, \frac{\beta}{t}, \dots\right) \quad . \tag{3.10}$$

It has been argued that the α term should vanish due to energy inversion symmetry.
The α' correction is suppressed by $t^{-1/4}$ and thus leads to a further summand $t^{-3/4}$. It appears for all three mass ratios for long times. For $N = 1$ the correction is nearly negligible for very long times which could not be observed in [2] for the numerics have been improved in the meantime. It could be explained by the fact that umklapp scattering becomes less important for longer times since most momenta are very similar by then and thus only few momenta have to be back-folded into the Brillouin zone. It can be seen that the correction becomes dominant for higher N. A disappearance of this correction for lower mass ratios can not be excluded. It would take better numerics and longer times to ascertain that.
In the region between 100τ and 200τ in all three cases a knee in the curve can be observed. Starting from a quite low time until reaching this knee the data can be fitted by a power law with way more deviation from $t^{-1/2}$. This deviation increases when decreasing the mass ratio. Thus it can not be explained by umklapp scattering as its effect should decrease (fig.11).

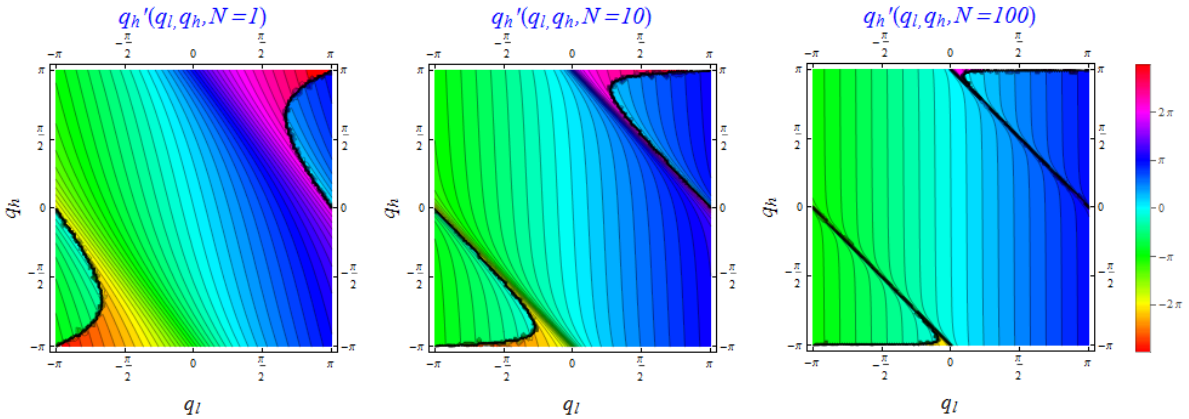

Figure 11: *New momentum of the particle which can do umklapp scattering after a scattering event in dependency of the both old momenta and before umklapp scattering has taken place. Umklapp scattering can happen if the new momentum's absolute value exceeds π. The higher N the lower the effect of umklapp scattering gets.*

It is indeed problematic to draw interferences from umklapp scattering to hydrodynamics.

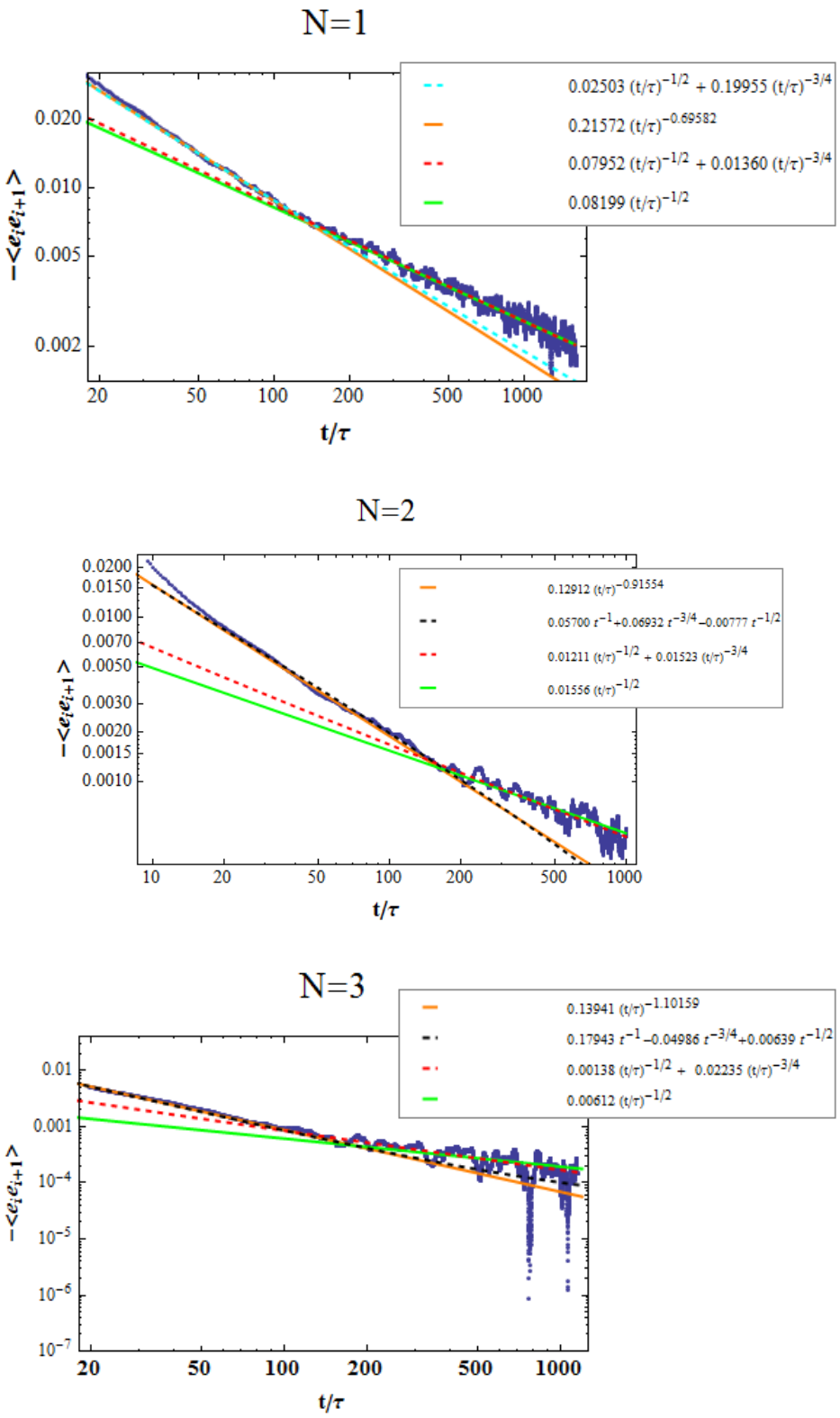

Figure 12: *Long-time behavior of the energy correlation for N=1,2,3 and fits for both regions in log-log plots. Averaged over 4, 16 and 20 scattering times. For every N the data is averaged over 1200 runs.*

For $N = 1$ a more pronounced $\sim t^{-3/4}$ correction caused by the α' term is sufficient. For $N = 1$ and $N = 2$ this is not the case. It can be seen that a further correction $\sim t^{-1}$ needs to be regarded. Following the scaling calculation this could be an effect of the β term. Still it does not explain why this correction seems to vanish at about $100\tau - 200\tau$. That could be an interesting question for future investigations.
Finally we want to compare the prefactors for long times and the different mass ratios. Thus we use the prefactors a_N of the long-time $t^{-1/2}$ fit and divide them. What we get is $\frac{a_1}{1_2} \approx 5.27 \approx 2^{2.40}$ and $\frac{a_1}{a_3} \approx 13.40 \approx 3^{2.36}$. The accordance can be coincidental or not for it is not possible to conclude something from two numbers. Later on the prefactors from $\cos(2q)$ long-time tails will be compared, too.

3.3 Momentum Distribution - A "Remembering" Quantity

The second quantity observed is $\langle\cos(2q)\rangle$ which can be associated with the shape of the momentum distribution. It starts from

$$\langle\cos(2q)\rangle(0) = \frac{1}{2}\int_{-\pi}^{\pi} \mathrm{d}q\, \cos(2q)p_0(q) = -\frac{1}{2} \tag{3.11}$$

and does not change its sign at any time. Concerning finite N this quantity relaxes to zero (eq.(3.16)) due to umklapp scattering. For same masses umklapp scattering does not appear any more for the momenta are just exchanged and thus the momentum distribution does not change. This is the quantity in which integrability is pronounced, beacuse thermalization declines until there is no thermalization left. In the following we will first observe the exponential decay which governs the behavior for short times $t < t_c$, where t_c increases for larger N, and afterwards investigate the long-time tails.

3.3.1 Exponential Decay

The exponential decay (see fig.13) can be described theoretically by the Boltzmann equation. The Boltzmann quation is a transport equation for distribution densities in dilute kinetical gases. We use the distribution functions of heavyons and lightons n_q^h and n_k^l with

$$n_q^h(0) = n_k^l(0) = n(0^+) \tag{3.12}$$

with $n(0^+)$ from 2.1.3. Concerning energy conservation as well as momentum conservation modulo 2π, the inversion symmetry $W_{k,q,k',q'} = W_{k',q',k,q}$ of the transition rate $W_{k,q,k',q'}$, which describes the probability density per time unit that particles with momenta q and k change their momenta by colliding to q' and k', and by making use of the Stoßzahlansatz the equations for both species become [2]

$$\begin{aligned}\partial_t n_k^l = \frac{1}{(2\pi)^3}\int_{-\pi}^{\pi}\mathrm{d}q\int_{-\pi}^{\pi}\mathrm{d}q'\int_{-\pi}^{\pi}\mathrm{d}k'\, W_{k,q,k',q'}\delta(\epsilon_k^l+\epsilon_q^h-(\epsilon_{k'}^l+\epsilon_{q'}^h))\\ \sum_{n\in\mathbb{Z}}\delta(k+q-(k'+q')+2\pi n)(n_{k'}^l n_{q'}^h - n_k^l n_q^h)\\ \partial_t n_q^h = \frac{1}{(2\pi)^3}\int_{-\pi}^{\pi}\mathrm{d}k\ \ldots\end{aligned} \tag{3.13}$$

where the equation for the heavyon distribution is the same as for the lighton distribution up to the change of integrals $\int_{-\pi}^{\pi}\mathrm{d}q \mapsto \int_{-\pi}^{\pi}\mathrm{d}k$. It is motivated by continuity of $\partial n/\partial t$ and thus $(\partial_t n)_{in} = (\partial_t n)_{out}$ As we have seen in 2.3 the product of both deltas is proportional to $\delta(k'-k_l)\delta(q'-(k+q-k_l))$ with k_l from eq.(2.23). Heuristically one can say that the probability that two particles scatter after time Δt is $\mathbb{P} \sim \frac{|\Delta v|\Delta t}{L}$ and thus $d\mathbb{P}/dt \sim |\Delta v|$. To guarantee the symmetry and right dimension the transition rate has to be $\sim |\partial_k\epsilon_k^l - \partial_q\epsilon_q^h||\partial_{k'}\epsilon_{k'}^l - \partial_{q'}\epsilon_{q'}^h|$. The

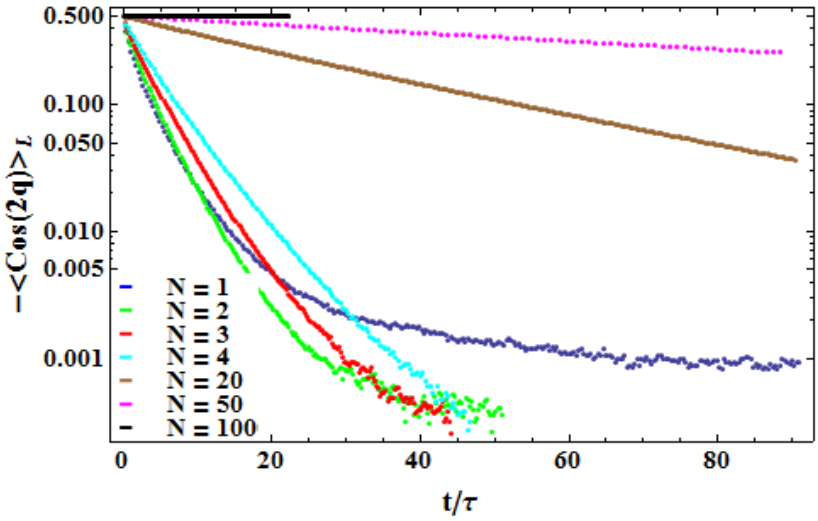

Figure 13: *Exponential decay of* $-\langle\cos(2q)\rangle_l$ *for various mass ratios in a log-plot. For N=1 the long-time tail part can already be seen.*

proportionality constant is $(2\pi)^2$. Using the delta's the transition rate becomes $W_{k,q,k_l,q+k-q_l}$. The probability for this crossing is one. Thus one receives $W_{k,q}$ where the q', k'-part vanishes. Noting "k or q" as (k, q) in the equations the distributions read

$$\partial_t n^{l,h}_{k,q} = \frac{1}{2\pi}\int_{-\pi}^{\pi} \mathrm{d}(q,k)\,|\partial_k\epsilon^l_k - \partial_q\epsilon^h_q|(n^l_{k_l} n^h_{k+q-k_l} - n^l_k n^h_q). \tag{3.14}$$

As n is periodic in the momentum with periodicity 2π one can expand n into a Fourier series

$$n^{l,h}_{k,q} = \sum_m \cos(m(k,q))a^{l,h}_m \quad .$$

The coefficients a_m are given by

$$a^{l,h}_m = \frac{2}{2\pi}\int_{-\pi}^{\pi} \mathrm{d}(k,q)\, n^{l,h}_{k,q}\cos(m(k,q)) \quad .$$

Inserting this into (3.14) yields to

$$\begin{aligned}\partial_t a^{l,h}_m &= \frac{1}{\pi}\int_{-\pi}^{\pi} \mathrm{d}(k,q)\,|\partial_k\epsilon^l_k - \partial_q\epsilon^h_q|\cos(m(k,q))(n^l_{k_l} n^h_{k+q-k_l} - n^l_k n^h_q)\\ &\overset{\text{Fourier}}{=} \frac{1}{\pi^2}\sum_{m',m''} a^{l,h}_{m'} a^{h,l}_{m''}\int_{-\pi}^{\pi}\mathrm{d}k\int_{-\pi}^{\pi}\mathrm{d}q\,\Big[\cos(m(k,q))\\ &\left|\frac{N+1}{N}\sin(k) - \sin(q)\right|\Big(\cos(m'k_l)\cos(m''(k+q-k_l)) - \cos(m'k)\cos(m''(q))\Big)\Big]\end{aligned} \tag{3.15}$$

as already calculated in [2] for $N = 1$. It shows that all modes with odd m vanish. In order to satisfy the initial condition (3.12) the $m = 0$ modes as well as minus the $m = 2$ modes are set to the density at $t = 0$. All other modes are set to 0 for this time. The $m = 0$ mode is constant

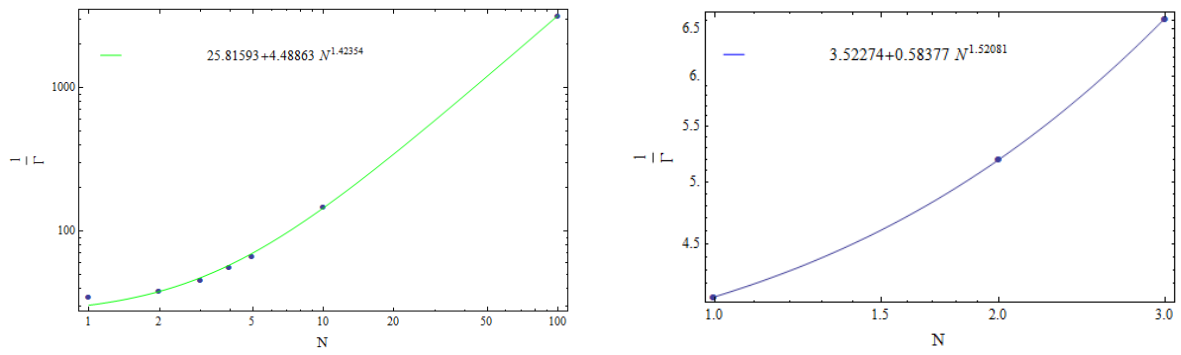

Figure 14: *Theoretical N-dependency of the decay of the m=2 mode concerning m=(0,2) modes (left) and m=(0,2,4) modes (right). (Boltzmann)*

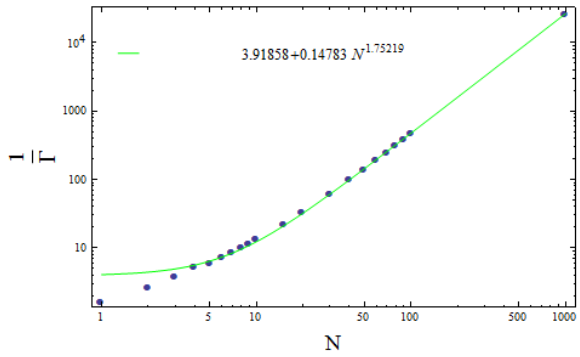

Figure 15: *Time scale of decay* $\frac{1}{\Gamma}$ *as a function of* N *obtained from the simulation.*

in time and all modes $m >= 4$ are very weak. Thus the $m = 2$ mode dominates the temporal behavior of n_k and therefore of $\langle \cos(2q) \rangle$.
In the simulation the exponential parts of $\langle \cos(2q) \rangle_l$ have been fitted with $0.5 \cdot e^{-t/\Gamma}$ for various N. The theoretical equation (3.15) for lightons has been solved numerically for $N = 1, 2, 3, 4, 5, 10, 100$ by only taking into account $m = 0, 2$ and for $N = 1, 2, 3$ by taking into account also $m = 4$. The resulting curves for the $m = 2$ mode have been fitted with $-0.0004 \cdot e^{-t/\Gamma}$ The results can be seen in fig.14 and fig.15.

The y-intercept in the simulated data is not needed but it does not make a noticeable difference if it is left out. One can see an general behaviour of $\sim N^{1.75}$. It does not fit very well for small N (neither does it by setting $\Gamma(0) = 0$) but from $N = 5$ up to $N = 1000$ it really shows this behavior. The half-analytical data's behavior approaches that of the simulated by including more modes to the calculation. Including even more modes and doing this calculation for more values of N should lead to an improved agreement with the simulated data.

3.3.2 Long-Time Tails

Long time tails do also appear in the $\langle\cos(2q)\rangle$. Since this quantity falls exponentially without a sign change before tails, they do fluctuate even faster around zero than the energy correlation. Again $N = 1, 2, 3$ are concerned but already for $N = 3$ the fits cannot be called good anymore. Prefactors can be compared but regarding the shape of the power-law it is already quite useless. As we one can see in fig.16 the difference of heavyons and lightons is the prefactor of the tails but the tails itself are quite parallel. Therefore only the curves of lightons will be shown. This quantity relaxes really with $t^{-1/2}$ and for higher N maybe with a correction $t^{-3/4}$ (fig.17). For $N = 1$ a small region could be associated with a further correction but as this does not repeat for other N it seems unlikely. Ratios of prefactors are $\frac{b_1}{b_2} \approx 4.305 \approx 2^{2.11}$ and $\frac{b_1}{b_3} = 11.5 \approx 3^{2.22}$ which is comparable to the ratios from the energy correlation's ratios. If one wants to extract an exponent, then it seems definitely to be between 2 and 2.5.

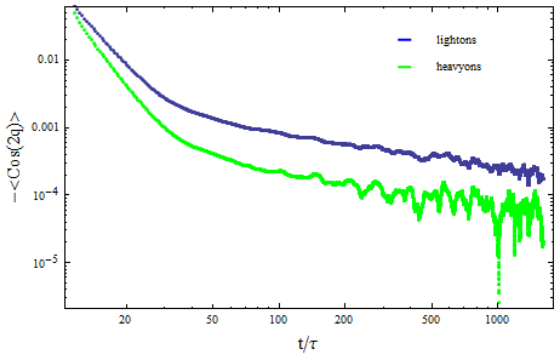

Figure 16: $\langle\cos(2q)\rangle$ *for heavyons (green), lightons (blue) and N=1*

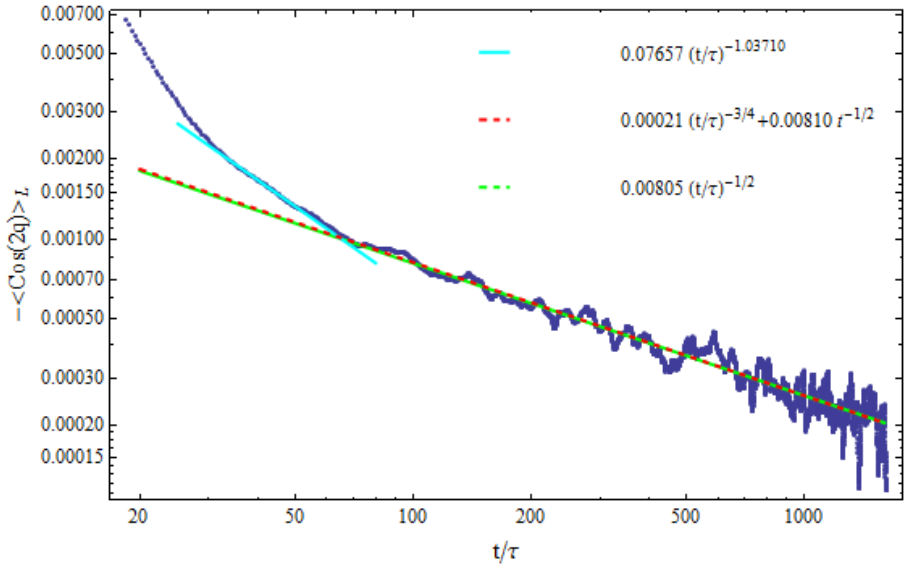

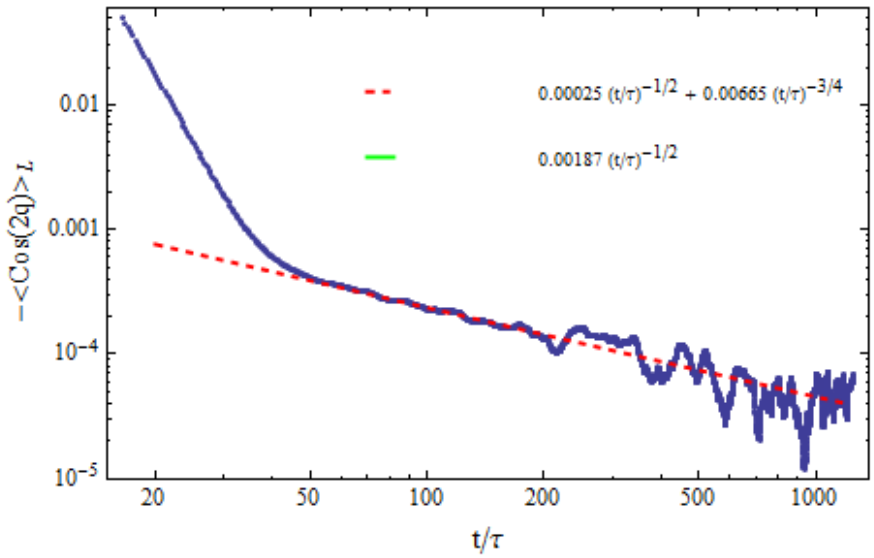

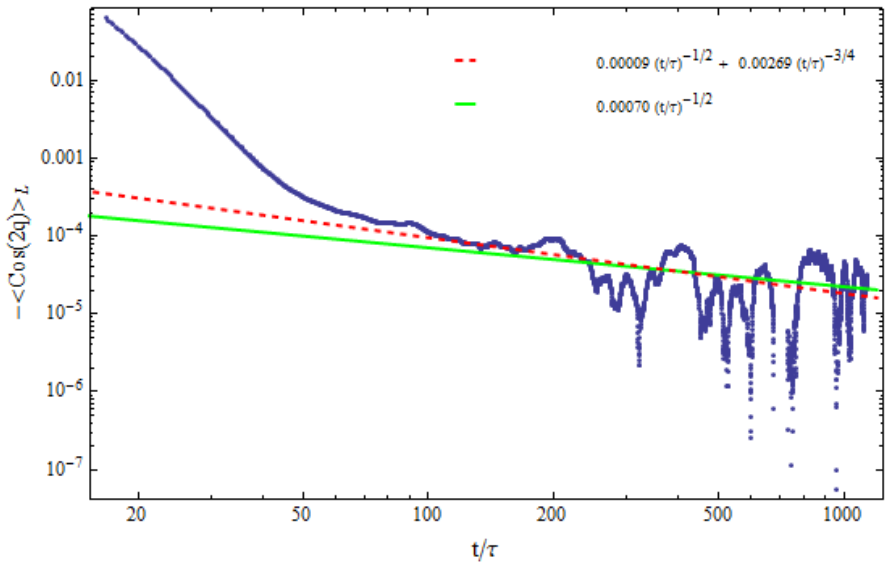

Figure 17: *Long-time tails of* $-\langle\cos(2q)\rangle_l$ *for N=1,2,3 (from top to bottom). Averaged over 10, 36 and 40 scattering times. For every N the data is averaged over 1200 runs.*

3.4 Comparison Near Equilibrium

Near equilibrium relative prefactors of the observed quantities can be compared for constant masses by doing a simple thermodynamical calculation. The total energy in the system vanishes

$$\langle e\rangle = \frac{1}{2}\Big(\int_0^\pi \mathrm{d}q \ \underbrace{\epsilon_l(q)p_0(q)}_{\sim\sin(q)\cos(q)} + \int_0^\pi \mathrm{d}q \ \underbrace{\epsilon_h(q)p_0(q)}_{\sim\sin(q)\cos(q)} \Big) = 0 \ .$$

Now one can use the thermodynamical definition of the energy's expectation value

$$\langle e\rangle(\beta, J, z_h, z_l, N) = \frac{1}{\langle n\rangle}\int_{-\pi}^{\pi}\mathrm{d}q \ \left(\epsilon_h z_h e^{-\beta\epsilon_h} + \epsilon_l z_l e^{-\beta\epsilon_l}\right) \quad ,$$

with the fugacities $z_{h,l}$ and the mean density

$$\langle n\rangle(\beta, J, z_h, z_l, N) = \int_{-\pi}^{\pi}\mathrm{d}q \ \left(z_h e^{-\beta\epsilon_h} + z_l e^{-\beta\epsilon_l}\right) \quad ,$$

furthermore introduce

$$\langle \Delta n\rangle(\beta, J, z_h, z_l, N) = \int_{-\pi}^{\pi}\mathrm{d}q \ \left(z_h e^{-\beta\epsilon_h} - z_l e^{-\beta\epsilon_l}\right)$$

and finally expand $\langle n\rangle$, $\langle \Delta n\rangle$ and $\langle e\rangle$ in powers of β. This is reasonable because the reached equilibrium state has effective temperature $T = \infty$, hence β can be considered a very small parameter near equilibrium.
Introducing the notation $\langle n\rangle(\beta, J, z_h, z_l, N) =: \rho$ and taking advantage of the same mean densities of heavyons and lightons, i.e. $\langle \Delta n\rangle = \langle n\rangle_h - \langle n\rangle_l = 0$, provides a system of two equations which allows to express z_h and z_l in terms of ρ, β and N

$$z_h(\rho, \beta, J, N) \quad , \quad z_l(\rho, \beta, J, N) \quad .$$

Inserting them into the energy yields to a dependency

$$\langle e\rangle(\rho, \beta, J, N) = \langle e\rangle(\beta, J, N)$$

as it emerges that the ρ-dependency vanishes. By inverting $\langle e\rangle$ one receives

$$\beta(\langle e\rangle, J, N)$$

and expand it in powers of $\langle e\rangle$.
The wanted observables then can be calculated as their thermodynamical expectation values

and expanded in powers of $\langle e\rangle$ again

$$\begin{aligned}\langle\cos(2q)\rangle_{l,h}(\langle e\rangle,J,N) &= \frac{1}{\langle n\rangle_{l,h}}\int_{-\pi}^{\pi}\mathrm{d}q\,\cos(2q)z_{l,h}e^{-\beta\epsilon_{l,h}}\\ \langle e_ie_{i+1}\rangle(\langle e\rangle,J,N) &= \frac{1}{8}\left(\frac{1}{\langle n\rangle_h}\int_{-\pi}^{\pi}\mathrm{d}q\,z_h\epsilon_he^{-\beta\epsilon_h}\right)^2+\frac{1}{8}\left(\frac{1}{\langle n\rangle_l}\int_{-\pi}^{\pi}\mathrm{d}q\,z_l\epsilon_le^{-\beta\epsilon_l}\right)^2+\\ &\quad\frac{3}{4}\left(\frac{1}{\langle n\rangle_h}\frac{1}{\langle n\rangle_l}\int_{-\pi}^{\pi}\mathrm{d}q\,z_h\epsilon_he^{-\beta\epsilon_h}\int_{-\pi}^{\pi}\mathrm{d}q\,z_l\epsilon_le^{-\beta\epsilon_l}\right)\quad.\end{aligned}$$

The prefactors $\frac{1}{8}$, $\frac{1}{8}$ and $\frac{3}{4}$ arise from a combinatorical consideration. Heavyons and lightons are always created together at neighbored sites with probability $\frac{1}{2}$ in the order heavyon-lighton and otherwise. The probability for the other neighbor to be one of the two species is $\frac{1}{2}$. Thus the probability to find HL (heavyon-lighton pair in this order) is $\frac{1}{2}\left(\frac{1}{2}+\frac{1}{4}\right)=\frac{3}{8}$ and the probability for LH is the same. Finally the probability for two neighbored particles to be different regarding their species is $\frac{3}{4}$ and to be the same $\frac{1}{4}$ which is symmetric for HH and LL, thus $\frac{1}{8}$ and $\frac{1}{8}$.
The results in second order of $\langle e\rangle$ are

$$\begin{aligned}\langle\cos(2q)\rangle_l &= \frac{1}{2}\left(\frac{\langle e\rangle}{J}\right)^2\frac{N^2(1+N)^2}{(1+2N+2N^2)^2}\\ \langle\cos(2q)\rangle_h &= \frac{1}{2}\left(\frac{\langle e\rangle}{J}\right)^2\frac{N^4}{(1+2N+2N^2)^2}\\ \langle e_ie_{i+1}\rangle &= \frac{1}{2}\left(\frac{\langle e\rangle}{J}\right)^2\frac{8N^4+16N^3+12N^2+4N+1}{(1+2N+2N^2)^2}\quad.\end{aligned}\tag{3.16}$$

Thus the relative coefficients are

$$g_N := \frac{\langle\cos(2q)\rangle_l}{\langle\cos(2q)\rangle_h} = \left(\frac{N+1}{N}\right)^2 = \left(\frac{m_h}{m_l}\right)^2 \tag{3.17}$$

$$f_N^l := \frac{\langle\cos(2q)\rangle_l}{\langle e_ie_{i+1}\rangle} = \frac{N^2(1+N)^2}{8N^4+16N^3+12N^2+4N+1}\quad. \tag{3.18}$$

It is mentionable that the only dependency of g_N is that of the ratio of masses $\frac{N+1}{N}$. For same masses g_N becomes 1 which means that near equilibrium the momentum distributions of heavyons and lightons are the same which does not surprise for they approach to become same-massed quasi-particles. Since the initial value of $\langle\cos(2q)\rangle$ does not depend on the masses and thus $g_N^{ini}=1$ the momentum distributions of the two species are nearly the same over all the time for a mass ratio near to 1.
The theoretical, relative coefficients can be compared to the simulation by considering the long-time tails and fitting them constantly $\sim t^{-1/2}$. This is not always a strictly true fit but it is sufficient in order to receive the approximate coefficients. Due to the statistical problems it is just possible for $N=1,2,3$ with the used number of particles and averaged ensembles. Noting the relative deviation as $\Delta_g := \frac{|g_N^{sim}-g_N^{theo}|}{g_N^{theo}}$ and analogue for f_N^l the results read

N	g_N^{theo}	g_N^{sim}	Δ_g	$f_N^{J,theo}$	$f_N^{J,sim}$	Δ_f
1	4	3.8188	4.53 %	0.0976	0.0983	0.75 %
2	2.25	2.2914	1.84 %	0.1150	0.1202	4.50 %
3	1.7778	1.6249	8.03 %	0.1200	0.1155	3.66 %

which is an acceptable accordance. The large relative deviation of g_3 is caused by the very low values of $\langle \cos(2q) \rangle_h$ which make it hard to fit a proper function to it.

4 Conclusion

It has been seen that the energy correlation does not decay exponentially for same masses but "relaxes" somehow more slowly. Some effect interferes with the correlation vanishing by a simple collision. Long time tails need a further, by now not observed correction $\sim t^{-1}$ which vanishes suddenly at a certain time.
Furthermore it has been observed that $\langle cos(2q)\rangle_l \sim e^{-at/N^{1.75}}$ which is not very far from the result of the Boltzmann equation regarding 0 to 4 modes. For same masses this quantity does not relax at all which shows the system's integrability. Relative prefactors of both quantities have been compared for constant mass ratio nearby an equilibrium state and show accordance with the numerical results within a relative deviation of 8 %.

References

[1] S. Sachdev and A.P. Young. Low temperature relaxational dynamics of the Ising chain in a transverse field. *Phys. Rev. Lett. 78, 2220*, March 1997.

[2] A. Mitra J. Lux, J. Müller and A. Rosch. Hydrodynamic long-time tails after a quantum quench. *Phys. Rev. A 89, 053608*, May 2014.

[3] F. Lange. Equilibrierung und Hydrodynamik in offenen Systemen. Bachelorarbeit, Universität zu Köln, 2014.

[4] I. Bloch. Ultracold quantum gases in optical lattices. *Nature Physics 1, 23 - 30*, 2005.

[5] F. Wilczek. Anyonen. *Spektrum der Wissenschaft*, July 1991.

[6] A. Altland and B.Simons. *Condensed Matter Field Theory.* Cambridge University Press, second edition, 2010.

[7] D. Fioretto. *Integrability and Out of Equilibrium Quantum Dynamics.* PhD thesis, International School For Advanced Studies, 2011.

[8] M. Rigol, V. Dunjko, and M. Olshanii. Thermalization and its mechanism for generic isolated quantum systems. *Nature 452, 854-858*, April 2008.

[9] S. Goldstein, J.L. Lebowitz, C. Mastrodonato, R. Tumulka, and N. Zanghi. Normal Typicality and von Neumann's Quantum Ergodic Theorem. *Proc. R. Soc. A 8 November 2010 vol. 466 no. 2123 3203-3224.*

[10] M. Möckel. *Real-time evolution of quenched quantum systems.* PhD thesis, Ludwig-Maximilians-Universität München, April 2009.

[11] J. Larson. Integrability vs Quantum Thermalization. *J. Phys. B: At. Mol. Opt. Phys. 46 224016*, November 2013.

[12] T. Kinoshita, T. Wenger, and D.S. Weiss. A quantum Newton's cradle. *Nature 440, 900-903*, April 2006.

[13] A. Hoffmann. Bosonen im optischen Gitter. Diplomarbeit, Freie Universität Berlin, 2007.

[14] H. Rieger and F. Iglói. Semi-classical theory for quantum quenches in finite transverse Ising chains. *Phys. Rev. B 84, 165117*, October 2011.

Appendix

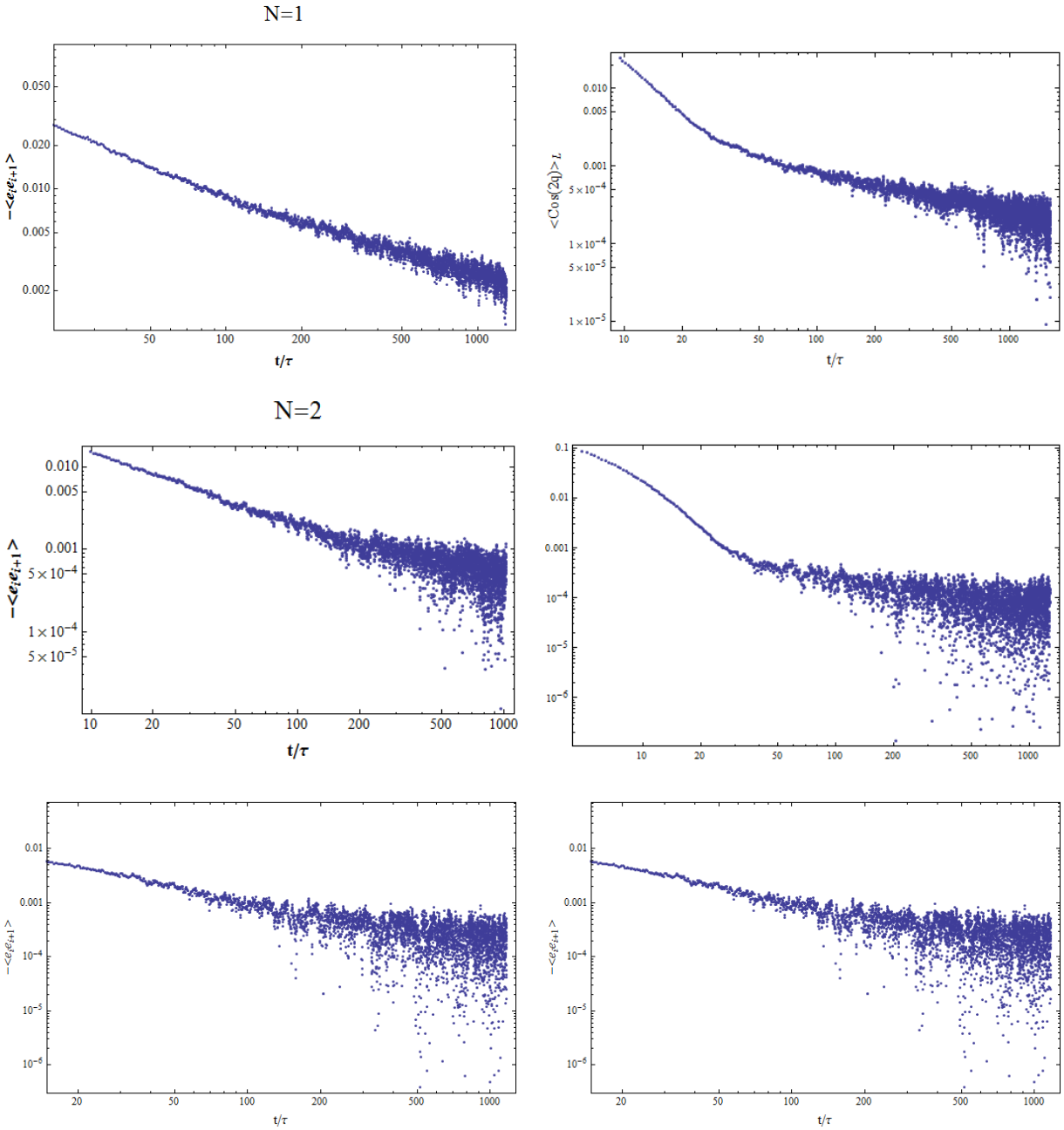

Figure 18: Data for $-\langle e_i e_{i+1}\rangle$ (left) and $\langle cos(2q)\rangle_l$ (right) for N=1,2,3 (from top to bottom) and without time-averaging in log-log-plots. In the left plot a time average is taken.

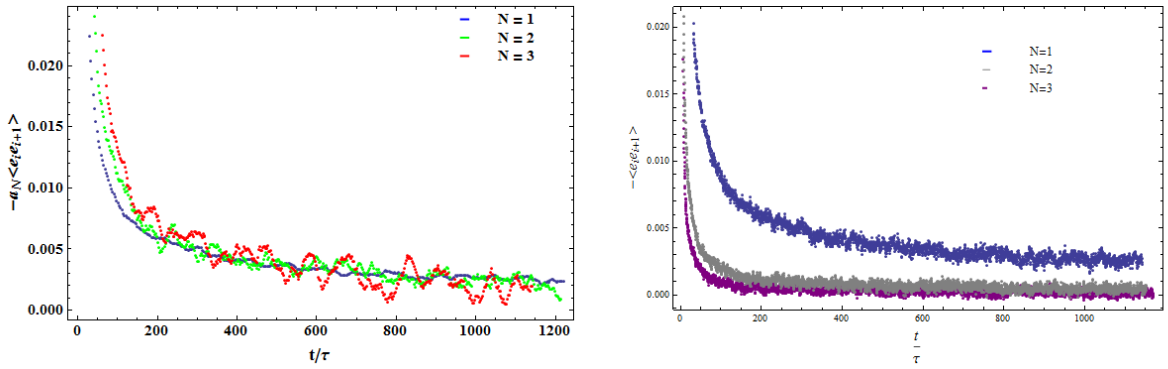

Figure 19: $-\langle e_i e_{i+1}\rangle$ for $N = 1, 2, 3$ raw (right) and multiplicated with $\frac{a_1}{a_N}$ (left) in linear plots.

Danksagungen

Ich möchte Herrn Prof.Dr. Rosch für die Auswahl des Themas, die Betreuung und die Möglichkeit, meine Bachelorarbeit in seiner Arbeitsgruppe zu schreiben danken.

Weiterhin bedanke ich mich bei Jonathan Lux, der das zur Simulation verwendete Programm geschrieben hat und den Großteil meiner Arbeit korrekturgelesen hat. Er stand mir stets mit Rat und Tat zur Seite und war immer ansprechbar. Desweiteren übermittelte er mir die Mathematica-Dateien zur numerischen Berechnung der theoretischen Gleichungen aus Kapitel 3.3.1 und 3.4. und half mir in 3.2.2.

Auch Florian Lange gebührt mein Dank, da er es durch die Bearbeitung des Programms ermöglicht hat, den abknickenden Verlauf der Energiekorrelationen zu beobachten. Er half mir bei numerischen Fragen immer weiter und ließ mich zu Beginn meiner Arbeit immer wieder an seinem bereits erworbenen Erfahrungsschatz teilhaben. Auch für das Lesen eines Großteils meiner Arbeit bedanke ich mich.

Zu guter Letzt möchte ich meiner Freundin Nikki dafür danken, dass sie mir die gesamte Zeit über zur Seite stand und großzügig über schlechte Laune und wenig Schlaf hinwegsehen konnte.

Eigenständigkeitserklärung

Hiermit versichere ich, dass ich die vorliegende Arbeit selbständig verfasst und keine anderen als die angegebenen Quellen und Hilfsmittel benutzt habe.

Datum, Ort: 17.07.2014, Köln .....

(Unterschrift)